Tomato Vines to Profit: Converting Harvest Waste into Green Energy, Fuels and Fertiliser

Vivienne Wells
Centre for Entrepreneurial Agri-Technology (CEAT), College of Science, ANU

Martin Amidy
Centre for Entrepreneurial Agri-Technology (CEAT), College of Science, ANU

Research report submitted to the

Australian Processing Tomato Research Council (APTRC)

Executive Summary

Waste processing tomato vines were gasified in a lab-scale reactor to quantify the yield potential of synthesis gas (syngas), which has varied uses as a renewable energy carrier or chemical feedstock. Pre-gasification analysis of the vines were undertaken to measure the chemical composition of the waste, which was used to simulate the thermodynamic equilibrium conditions of gasification in different conditions. Gasification with carbon dioxide (dry gasification), and steam were undertaken, and the syngas yield measured under varied oxidiser-to-biomass ratios. Modest yields of hydrogen were obtained from the process, the highest yield produced during gasification and downstream conversion of the carbon monoxide was 77 kg per tonne of tomato vine. The results from this project suggest that gasification of vine waste to produce hydrogen as a valorisation pathway would not be economically viable. This is due to low yields, high harvesting cost and the on-going decline in the cost of production for electrolysis technologies as primary source of global green hydrogen production.

Contents

List of Acronyms

APTRC	Australian Processing Tomato Research Council
Ar	argon
C	carbon
CH_4	methane
CO	carbon monoxide
CO_2	carbon dioxide
CSE	Concentrated solar energy
DI	deionised
DMFC	direct methanol fuel cell
FT	Fischer–Tropsch
GHG	greenhouse gases
H_2	hydrogen
H_2O	steam
HFC	heliostat field collector
HTC	hydrothermal carbonisation
LFR	linear Fresnel reflector
N_2	nitrogen
NH_3	ammonia
O_2	oxygen
PDC	parabolic dish collector
PEMFC	proton exchange membrane fuel cell
PTC	parabolic trough collector
RWGS	reverse water–gas shift
SMR	steam methane reforming
syngas	synthesis gas
TG	thermogravimetry
TGA	thermogravimetric analysis
WGS	water-gas shift

List of Figures

1 Introduction

The current climate and energy crises highlight the need to transition to clean and secure energy and process inputs. Whilst the agricultural industry is considered a hard-to-decarbonise sector, it also holds significant potential to contribute to a clean-energy future. Of particular interest is the use of waste streams such as renewable biomass, which can provide Australian producers with both an on-farm energy source and a potential income stream. Technological advances which increase the techno-economic feasibility of waste processing mean the use of recycled fuels will be increasingly beneficial to close the carbon loop and decrease our dependence on fossil-fuels [1]–[3].

Waste management for Australian farmers represents a significant challenge to balance the operational costs of primary production, disease mitigation, and sustainability. As the demand for renewable energy rises, and dependence on fossil-fuels and synthetic fertilisers carry higher risk, using organic waste streams as feedstocks for high-value products is also becoming a more viable option to diversify on-farm income streams [1], [2], [4].

Biomass is a renewable fuel source that can provide low-carbon energy in forms that can be used by existing systems and infrastructure with little adaptation. However, combustion of biomass has a low conversion efficiency into useful forms of energy, and its low energy density means that transportation becomes technically and economically prohibitive. Thus, biomass resource must be converted into more useful forms of energy to make its use techno-economically feasible. Waste tomato vines, a source of renewable biomass, contain roughly 14.8 GJ/ton, which can be harvested in various ways to provide useful energy [5]. Whilst the organic waste is often burnt in the paddock to prevent disease propagation through subsequent crops, this contributes to greenhouse gases (GHG) emissions and does not capture any of the energy in the biomass. Collection and combustion of the biomass is a well-known and commercial process but has a low conversion efficiency as much of the energy is lost to waste heat. Additionally, the low energy density of raw biomass compared to other fuels limits its usefulness across applications and makes transportation technically and economically prohibitive [6]. For utilisation of the waste streams to be economically viable, the value of the waste must exceed the cost of collection, transportation and handling, necessitating value-adding downstream processes.

It is possible to process the vine waste to "upgrade" the energy in the biomass into more useful forms of energy, gasification is an example of one of these processes. Gasification occurs when the biomass is heated under a controlled atmosphere to decompose the molecular structure of the biomass and release the carbon (C), hydrogen (H_2) and oxygen (O_2) it contains. The operational conditions under which gasification is performed can vary, including in the source and temperature of the heat provided, the reactor design, and the gases that are present in the reactor during the process. These factors can also impact the types and ratios of the products that are formed in the reaction, with the desired products being a mixture of H_2 and carbon monoxide (CO), called synthesis gas (syngas) [7].

Syngas is currently of particular interest and can be used in a downstream process to synthetic liquid hydrocarbon fuels like methanol, kerosene (jet fuel) and diesel [8], [9]. The syngas can also be used as a source of H_2, which is both a highly efficient energy carrier and vital for industrial processes and inputs, including ammonia and other synthetic fertilisers [10]. An additional product of gasification is a carbon char that has potential as an organic

soil amendment, which can increase soil-moisture retention and improve soil structure [11]. Similarly to the syngas, the composition of the biochar that is produced during the process depends on the feedstock and the process parameters used during gasification [11].

Gasification of waste tomato vines could therefore close the loop for carbon waste during growing processing tomatoes, potentially allowing for improved sustainability and cash-flow outcomes for Australian farmers. A schematic of the potential closed loop is shown below in Figure 1.

Significant improvements of gasification technologies are currently underway, with many different reactor designs and feedstocks being investigated. However, the technical and economic feasibility of any pilot plant is dependent on the type and volume of syngas that can be produced from the waste available in a specific region. Thus, the yield potential of syngas and its composition obtained when gasifying tomato vines must be determined to further assess the viability of post-harvest waste utilisation in this way.

In this project, members of the Australian Processing Tomato Research Council (APTRC) harvested tomato waste shortly after fruit harvest at three different locations within the growing region. The vine was analysed to determine its physical properties, including moisture content, ash yield and elemental constituents. The samples were then processed and gasified in a lab-based reactor under carbon dioxide (CO_2) and steam (H_2O) oxidisers, with the composition of the liberated gases measured and recorded at small time intervals.

From these data, the yield and composition of the syngas produced during the gasification process under various biomass-to-oxidiser ratios was calculated, which was extrapolated to understand the production potential of an entire harvest's waste under various processing scenarios. The outcomes of this project will be an important contribution to understand the potential to convert waste agricultural streams into high-value, low-emissions products to diversify income streams and increase the overall profitability and resilience of Australian processing tomato growers.

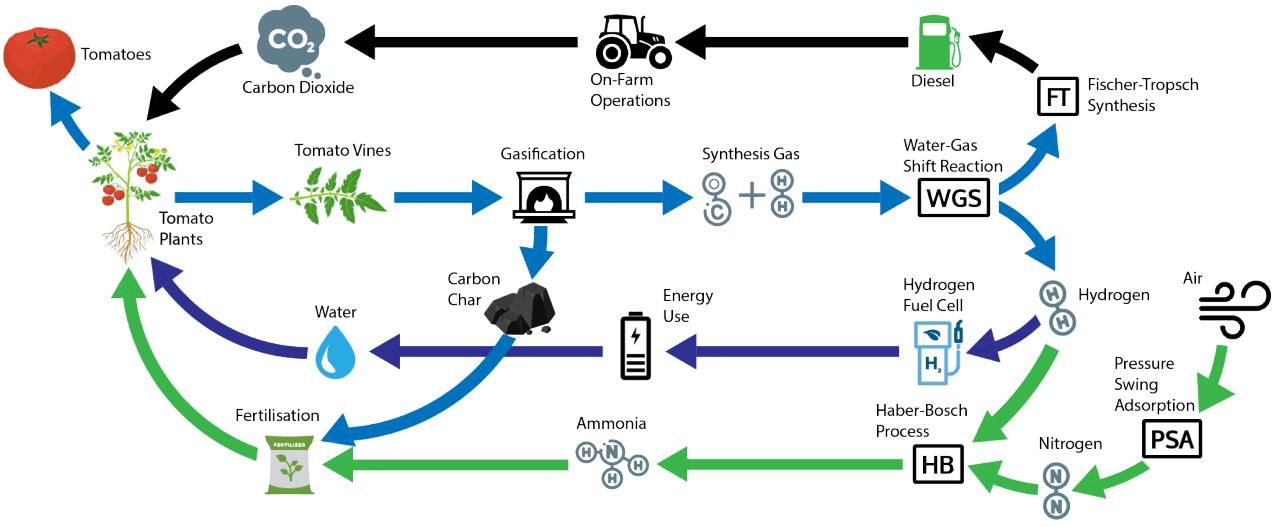

Figure 1: Recycling carbon and hydrogen through tomato production. Showing synthetic fuel production (top), hydrogen use as an energy carrier (second from bottom), and fertilisation with ammonia (bottom)

2 Background

Competition with cheaper, imported tomato products means that Australian growers have faced shrinking market share at the same time as production costs have significantly increased [5]. Whilst increasing the efficiency of fruit production volumes is a topic of interest in the industry, it does not sufficiently increase the competitiveness of farmers in the Australian market and so the addition of other income streams for farmers should be investigated [5].

Henry, identified a potential pathway to new revenue opportunities through gasification of harvested waste tomato vine in his 2018 Nuffield Scholarship report [5]. The total mass of vines remaining in paddocks after the harvest of processing tomatoes is estimated to be 25 000 tons each season, which could be collected for gasification [5]. To investigate this pathway monetising tomato vine waste, the APTRC has funded this project to quantify the resource level obtained during gasification of the waste at the end of a harvest.

2.1 Gasification

The trend toward sustainable energy sources in the past several decades has been accompanied with a great increase in the interest of using biomass as a carbon neutral fuel source [12], [13]. This has been accompanied with an exponential growth in research into biomass gasification, which is seen as one of the most important routes for biomass energy conversion [12], [13]. Over the last two decades 8698 articles on biomass gasification were published on the ScienceDirect website, 20% of these being published in the *International Journal of Hydrogen Energy* and *Energy* journals [13]. This demonstrates the importance of biomass gasification in the energy transition and as a process to create green hydrogen.

Currently, gasification of carbon-rich materials, most commonly coal, is a common procedure to produce H_2 as an industrial feedstock [7], [14]. The reaction is performed at temperatures above 570°C and uses air, O_2, H_2O or CO_2 as an oxidising agent, which drives the thermodynamic equilibrium toward CO and H_2 [7], [13]. Whilst partial oxidation with air and O_2 reduces the heating requirements of the reaction, the syngas that is produced is lesser in quality and energy efficiency than when using H_2O and CO_2, with use of the latter being of interest to use an additional carbon stream in the process [12], [13].

Biomass, being an overarching term, includes a large number of materials and therefore has different molecular compositions [15]. However, in order to understand the thermodynamics of reactions, simplified net reactions for gasification are often used and those for steam and dry gasification are shown below in Equations 1 and 2, respectively.

$$CH_xO_y + (1-y)\,H_2O \rightarrow \left(\frac{x}{2} + 1 - y\right) H_2 + CO \quad (1)$$

$$CH_xO_y + (1-y)\,CO_2 \rightarrow \frac{x}{2} H_2 + (2-y)\,CO \quad (2)$$

Whilst syngas is the end product of the net reaction, there are several intermediate reactions that occur, shown below in Equations 3 – 5, producing intermediate products that may not

be fully converted to CO and H_2 during the residence time of the gases in the reactor [7].

$$C + HO_2 \rightleftharpoons 2CO \quad (3)$$

$$C + 2H_2 \rightleftharpoons CH_4 \quad (4)$$

$$CO + H_2O \rightleftharpoons CO_2 + H_2 \quad (5)$$

The most notable of these is methane (CH_4), which is undesirable for several downstream processes using the syngas [14]. Thus, the methane present during gasification should be reformed to create additional CO and H_2. Whilst methane reforming is also a topic of great research interest, for the purposes of this study it can be assumed that complete conversion of the methane to CO and H_2 is achieved [10].

During steam gasification —- where steam is used at the gasifiying agent —- higher amounts of H_2 are produced due to the addition of the H_2 contained in the steam to the reaction when compared with dry gasification where CO_2 is the oxidiser [7].

As most uses of syngas require larger volumes of H_2 than CO, the amount of H_2 produced can be increased by reacting the CO in the product gases with H_2O through the water-gas shift (WGS) reaction, with a byproduct of CO_2 [7]. This can be fed back into the gasifyer if dry gasification is being undertaken, be used as a feedstock for chemical processes requiring CO_2 such as urea production, stored as a form of carbon sequestration, or released into the atmosphere. As this CO_2 would be derived from the waste tomato vines in the case of steam reforming, the emission of this stream into the atmosphere would be carbon neutral as it was initially captured from the atmosphere during photosynthesis undertaken by the tomato plant [16].

There is intense research on how the process parameters affect the yield and quality of syngas that is produced [12], [13]. These include the type of biomass feedstock, reactor type and configuration, gasification agent used, temperature, pressure, biomass pre-processing and particle size, and oxidiser-to-biomass ratio [12], [13], [15]. These factors influence the overall efficiency of the process, as well as the amount of H_2, CO, methane, tar and biochar produced during gasification [13].

Biomass sources have vastly varied types and elemental composition, meaning that the syngas produced can be of greatly different amounts and qualities [15]. Understanding the properties of the syngas that is produced from available biomass sources is important to scope the potential yields from gasification of different feedstocks, as well as the possible improvements to the composition upon co-gasification with other types of biomass [15]. Co-gasification of distinct biomass materials has been found to increase the energy and biomass-use efficiency of the process [15].

The extent of gasification and the resulting syngas and biochar composition is found to vary greatly with the oxidiser-to-biomass ratios [13]. In steam gasification, higher steam-to-biomass ratios lead to higher conversion efficiencies of the biomass, reduced tar formation and high H_2 content [13]. However, very high steam-to-biomass ratios can lead to the formation of methane and other hydrocarbons due to lower reactor temperatures that can

be caused by high oxidiser flow rates in practical applications [13]. Additionally, the energy requirements and cost of providing excess steam to the reactor is high due to the high specific heat capacity and latent heat of H_2O [13]. Gasification is undertaken at high temperatures, with the necessary heat normally provided by burning a portion of the feedstock or products in industrial plants [17]. This decreases the overall yield of syngas, and so other sources of renewable heat are advantageous to provide this process heat. Concentrating solar energy is of particular interest in this field as it is able to provide the very high temperatures that are needed for these reactions, and gasification reactors are some of the most mature solar thermochemistry reactor concepts [7].

Whilst the reactor design is an important consideration for the commercialisation of gasification processes, it is outside of the scope of this research and so the results of using a lab-scale down-draft reactor is considered sufficient to compare the syngas yield and quality from tomato vines. Additionally, temperature, pressure, biomass pre-processing and particle size is not investigated.

2.2 Uses for Gasification Products

A variety of products can be produced during downstream processing of syngas, or alternatively it can be used directly as a combustion fuel [10], [14]. These include H_2 and ammonia (NH_3), methanol and synthetic liquid hydrocarbon fuels through the WGS and separation, the Haber-Bosch synthesis, and the Fischer–Tropsch (FT) synthesis, respectively.

2.2.1 Hydrogen

H_2 can be used in a variety of ways as an energy carrier or chemical feedstock. As a fuel, it can be combusted in a gas turbine or undergo electrochemical reactions with oxygen in a fuel cell to generate electricity directly. The only product of both of these processes is water, as shown in Equation 6, making H_2 a zero-emissions fuel and of particular interest for the energy transition [18]. Currently, technical and economic challenges around its use to replace liquid fuels in heavy industry, but it is forecast to be a key commodity in a decarbonised future [18].

$$2H_2 + O_2 \rightleftharpoons 2H_2O \tag{6}$$

The majority of the world‘s H_2 supply, contributing to approximately 76% of the world‘s supply, comes from steam methane reforming (SMR), which uses natural gas, a fossil fuel as the main feedstock in the reaction shown in Equation [19].

$$CH_4 + H_2O \rightleftharpoons CO + 3H_2 \tag{7}$$

As the natural gas is a fossil fuel, this process contributes to GHG emissions and therefore renewable sources of H_2 are being investigated intensively to build a carbon-neutral H_2 supply chain [19]. The use of renewable feedstocks, in particular water and waste biomass, is being advanced to bring down the costs of converting these materials into H_2 in line with the current cost of SMR [18], [19].

Whilst H_2 is produced in biomass gasification, the syngas produced also contains large quantities of CO. In order to increase the production of H_2 from biomass, this CO should be reacted with H_2O in the WGS reaction (Equation 5).

Fuel cell are electrochemical devices that convert the chemical energy stored in H_2 into electricity through two half cell reactions, which have the overall reaction shown in Equation 6 [20]. The half cell reactions differ depending on the type of fuel cell that is used [20]. The most common type of fuel cells used are proton exchange membrane fuel cell (PEMFC), which use a polymer electrolyte and platinum electrodes to perform the reactions shown in Equations 8 and 9 at the anode and cathode, respectively [20].

$$H_2 \rightarrow 2H^+ + 2e^- \tag{8}$$

$$O_2 + 4H^+ + 4e^- \rightarrow 2H_2O \tag{9}$$

Fuel cells exhibit higher energy efficiency than combustion engines, with PEMFCs operating between 40–55% [21]. In comparison, most commercial gas turbines operate between 20–40% efficiency [22].

Storage and transportation of H_2 is a current technological challenge that is currently being heavily investigated to make H_2 use cheaper and more sustainable [23]. Whilst H_2 contains a lot of chemical energy per unit weight, it has a low volumetric energy density, meaning it needs a lot of space to transport and store [23]. Thus, it is compressed, liquefied or adsorbed onto solid storage media, with the latter still in the developmental stage of the technology [23].

Compression is the most common form of storage preparation, as it is simple and relatively fast, meaning cheaper materials and infrastructure can be used [23]. However, the volumetric energy density of liquid H_2 is much higher than that when it is compressed. Liquid H_2 must be stored at temperatures below −253°C, meaning insulated containers are required to keep the H_2 in its liquid form [23]. Both compression and condensation of H_2 to store and transport use a large amount of energy, decreasing the overall energy efficiency of H_2 fuel utilisation.

2.2.2 Ammonia

The technological challenges to use H_2 as a commercial energy carrier mean that transformation of H_2 to other energy carriers is of interest. One such energy carrier is ammonia, which has a higher volumetric density and is easier to condense than H_2, and is of great interest to the maritime sector [24]. Currently, ammonia is predominantly used for synthetic fertilisers for agricultural production and its production accounted for 1.3% of CO_2 emissions in 2020 [24]. To create ammonia, H_2 is reacted with nitrogen (N_2) at high temperature and pressure during the Haber-Bosch process, as shown in Equation 10 below [25].

$$3H_2 + N_2 \rightleftharpoons 2NH_3 \tag{10}$$

As N_2 makes up approximately 80% of the earth‘s atmosphere, it is relatively inexpensive to extract it from air, meaning that the bulk of the production cost and emissions from

creating ammonia is from obtaining the H_2, as well as the high operating temperatures and pressures [26]. Whilst other methods of ammonia synthesis are being investigated, the Haber-Bosch synthesis is likely to remain the industrial standard for the immediate future and so decreasing the cost and GHG emissions intensity of the H_2 feedstock is necessary [26].

There is a huge demand for ammonia-based fertilisers in Australia, with over 3.9 million tonnes of nitrogen fertiliser on the market annually [27]. Currently, China produces about 30% of the world's ammonia supply, with the European Union, India, the Middle East, Russia and the United States produces between 8–10% each [28]. With ongoing global trade instability and Australia's large potential to produce low-cost renewable energy, there is significant interest in increasing local production of "green ammonia" with renewable sources of H_2, such as that from waste biomass gasification [29].

Urea-based fertilisers are the biggest user of ammonia, with about 57% of the ammonia produced globally used for urea production [28]. Commercially, urea is produced in two steps, producing ammonium carbamate through the Bazarov reaction, which is then dehydrated to obtain urea [30]. These reactions are shown in Equations 11 and 12 below [30].

$$CO_2 + 2NH_3 \rightarrow NH_2COONH_4 \tag{11}$$

$$NH_2COONH_4 \rightarrow NH_2CONH_2 + H_O \tag{12}$$

2.2.3 Methanol

Methanol is one of the most important chemical commodities, with rapid growth in its demand [31]. It is also considered as a possible renewable fuel and replacement raw material to replace many fossil-fuel chemical feedstocks [32], [33].

Methanol synthesis is undertaken at temperatures between 200–300°C and pressures of 50–100 bar, and currently uses fossil-derived syngas [32], [33]. The synthesis involves the reactions shown below in Equations 13 and 14, along with the reverse water–gas shift (RWGS) in Equation 15 [32].

$$CO + 2H_2 \rightleftharpoons CH_3OH \tag{13}$$

$$CO_2 + 3H_2 \rightleftharpoons CH_3OH + H_2O \tag{14}$$

$$CO_2 + H_2 \rightleftharpoons CO + H_2O \tag{15}$$

As Reaction 14 produces water as a byproduct, and the RWGS (Equation 15) consumes energy and produces CO_2, Reaction 13 is the preferred synthesis route. This means that the desired ratio of H_2:CO in the syngas feedstock is 2:1.

Methanol has many advantages over H_2 as a fuel, being easier to handle, having a higher volumetric energy density and being a more direct substitute for oil products in the chemical

industry [31], [33]. Whilst methanol can be blended with gasoline, it can also be used neat as a transportation fuel, with 40% of the total methanol produced being used this way in a China [31], [34]. However, methanol can also be used to generate electricity directly in a direct methanol fuel cell (DMFC), similarly to hydrogen fuel cells described above [31]. The half-cell and overall reactions in a DMFC are shown below in Equations 16 – 18 [31].

$$\textit{Anode:}\ CH_3OH + H_2O \rightarrow CO_2 + 6H^+ + 6e^- \tag{16}$$

$$\textit{Cathode:}\ \frac{3}{2}O_2 + 6H^+ + 6e^- \rightarrow 3H_2O \tag{17}$$

$$\textit{Overall:}\ CH_2OH + \frac{3}{2}O_2 \rightarrow CO_2 + 2H_2O \tag{18}$$

DMFCs currently have a relatively low efficiency of less than 30% due to technical challenges and so are mainly used in for portable power generation in niche markets such as military applications [31], [35], [36]. However, as there is much less energy required for the storage and transportation of methanol compared to H_2, the overall efficiency of electricity generation with DMFCs is not vastly different from hydrogen fuel cells [31]. With further innovation in fuel cell technologies, the efficiency of DMFCs is expected to increase significantly, which will drive increased used of DMFCs and methanol as a fuel [35], [36].

2.2.4 Synthetic Liquid Fuels

The FT process is a commercially mature process that has been producing synthetic fuels since the 1930s [8], [9]. Whilst interest in the production of fuels through FT synthesis has fluctuated historically with fluctuations in the price of crude oil, there has been a resurgence of interest in the process due to the need to produce carbon-neutral fuels for use in hard-to-decarbonise sectors such as aviation [37].

Alkanes of various chain lengths are synthesised through the FT process, with the length of these chains controlled by adjusting the H_2:CO ratio and reactor parameters such as time on stream and operating temperature and pressure [37]. The production of alkanes, including those contained in kerosene and diesel is shown in Equation 19 below [37], [38].

$$(2n + 1)H_2 + nCO \longrightarrow C_nH_{2n+2} + nH_2O \tag{19}$$

The average ratio of H_2:CO for this reaction is 2.1:1, meaning the ratio of in the feed syngas is usually adjusted after production through the WGS reaction (Equation 5) [8], [37].

The synthetic fuels produced have the same chemical composition as those derived from crude oil and can be used in existing technologies [8], [37]. Whilst the FT synthesis is a well-known commercial process, it is currently not economically competitive with fuels derived from crude oil, with the largest contributor to its cost being the production of the syngas [8]. Thus, cost effective sources and production methods of renewable syngas are being heavily investigated.

2.2.5 Biochar

Biochar has received increasing attention in recent years for a variety of applications, including carbon sequestration and soil remediation and amelioration [11], [39]. Biochar is a carbon-rich material produced from organic feedstocks and has advantageous properties such as high carbon content, large specific surface area, high cation exchange capacity and stable molecular structure [11].

The sustainable processing and disposal of many organic waste streams, including sewage sludge and agricultural wastes is a global challenge [11]. The production of biochar from these waste streams has the possibility to safely process these waste streams, reduce emissions from their disposal, sequestering their carbon in a stable state, and provide improvements to soil quality when used as a soil additive [11], [39].

Biochar can be produced through a range of processes including pyrolysis, gasification and hydrothermal carbonisation (HTC) [11], [39]. Similarly to the composition of syngas, the properties of biochar derived from different feedstocks and processes can vary greatly [11], [39]. As the gasification process is usually optimised for the production of syngas, the yield of biochar from this process is considerably lower than obtained during pyrolysis and HTC, being approximately 5–10% of the biomass used [39].

Biochar has been used for various purposes for thousands of years including heat and power generation, soil fertilisation, gas and water purification, and carbon sequestration [39], [40]. The high specific surface area and chemical properties of biochar make it an ideal adsorbent, being used to remove heavy metals in water and soils, and formaldehyde in air [39]. Additionally, the removal of many organic pollutants in soils, including polycyclic aromatic hydrocarbons which are toxic to mammals and aquatic life, can be conducted with biochar, with the success of the removal depending on biochar feedstock, production process and applied dose, and the pollutant targeted [11].

Biochar has been to promote plant growth in agriculture by increasing the total carbon, nutrient retention and availability, microbial activity, and soil moisture holding and permeability [41]. Its application has also been observed to alter soil pH, in some cases negatively, although the combined effects of biochar application has led to over two times production yield of crops in Australasia, China and South America [41]. Carbon sequestration is a biochar use of increasing interest due to the need to remove CO_2 from the atmosphere [11]. The carbon in biochar is relatively stable due to the resistance to biodegradation, which makes it an ideal sequestration medium due to its relative permanence [11]. Therefore, the use of biochar as a soil additive would benefit GHG emissions due to increased uptake of CO_2 with higher biomass yields, decrease post-harvest burning, which destroy soil organic carbon stocks, increase renewable energy use, and decrease the rate of decay of carbon-based soil products [42].

Whilst biochar shows promise as a soil amendment, its widespread use is partially limited by incomplete data about its effect on crop yields, environmental impacts, and soil organic carbon and quality [41], [43]. Further investigation on optimisation of biochar properties for different applications, and the holistic impact of its use in agriculture must be carried out on a widespread scale [43]. These factors are outside of the scope of this report.

2.3 Concentrating Solar Energy Systems

Solar energy is an attractive renewable energy sources for a variety of reasons including the surplus of the sun‘s energy that is incident on the earth‘s surface source [7]. More energy is provided on earth from the sun in an hour than is consumed here in an entire year [44].

Concentrated solar energy (CSE) uses reflectors to focus the energy of the sun on a receiver to use the heat in a reactor, energy cycle, or stored in a medium such as solar salt [10]. Commercially, four reflector and receiver arrangements are used: parabolic trough collector (PTC), parabolic dish collector (PDC), linear Fresnel reflector (LFR), and heliostat field collector (HFC). These systems are shown below in Figure 2.

The high temperatures required for gasification mean that only HFCs and PDCs are able to provide sufficiently high levels of heat [46]. As PTC and LFR systems exhibit lower concentration ratios, they usually operate at temperatures below 500°C [10], [44].

HFC systems are the newest commercial CSE technology are installed in few locations world-wide [44]. The system consists of a vast array of flat or slightly concave mirrors that track the sun on two axes to reflect its rays onto a receiver located at the top of a fixed tower [44], [47]. The heat collected at the receiver can reach operating temperatures of between 300 and 2000°C and can be used in a reactor, power cycle, or exchanged into transport or storage media [44]. Some systems feature a secondary reflector at the top of the tower, permitting the receiver to be located on the ground, improving the practicalities of the heat uses and the concentration ratios in the system [44]. HFC plants are usually large in order to achieve economies of scale required due to the high start-up costs of the technology [44].

PDCs are also able to reach sufficient temperatures for gasification reactions and are much more modular in their construction. They consist of a parabolic mirror that reflects the sun‘s rays onto a single point above the dish‘s centre, allowing very high concentration ratios and operating temperatures between 150–1500°C [44], [47]. The entire dish system follows the sun on a finely tuned two-axis tracking system to keep the mirrors‘ focal point on the

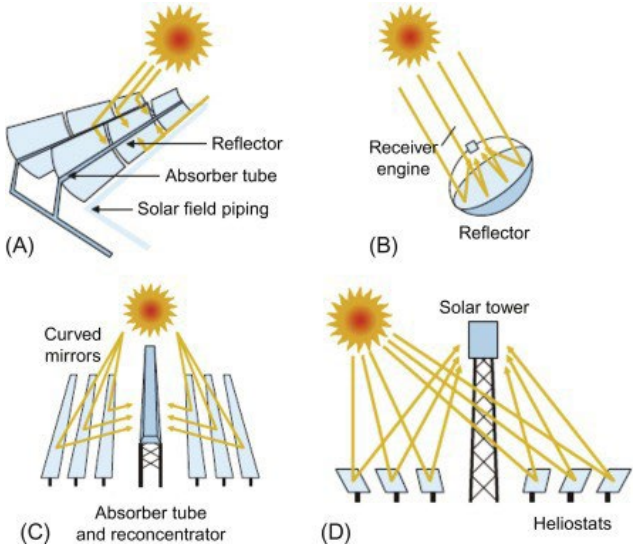

Figure 2: Schematics of current commercial CSE systems. (A) PTC; (B) PDC; (C) LFR; (D) HFC [45]

receiver, and the mirror must be precisely concave to effectively concentrate the radiation on the receiver [44]. These factors increase the manufacturing costs of the PDC system, although dishes have been trialled consisting of an array of many mirrors approximating a parabolic dish to reduce the upfront costs of these systems [44]. Additionally, these systems provide a modular alternative to the vast HFC systems, which may be useful in gasification operations where local biomass supply may be limiting [44].

The design of a pilot or commercial gasification plant would depend on a large range of factors, but these CSE systems provide an important alternative to tradition reactor systems. The use of these renewable energy systems would mean that no biomass or fossil fuels would need to be used to provide the heat to the gasification reaction, maximising the yield and sustainability of the process.

3 Experimental Procedure

3.1 Biomass Preparation

Samples taken from the paddock post-harvest were transported to the lab in moisture-proof containers in order to maintain the moisture content of the harvested samples for testing. The mass of the wet biomass was recorded when received and then dried at 80°C until there was no change in the sample mass between measurements. Biomass milling to create particle sizes with a mean diameter of 1 mm, 4 mm and 10 mm was investigated. However, it was found that due to the heterogenous nature of the vine material, which included tough vine and root material, as well as brittle leaf and fruit material, milling it to different sizes meant that the resultant samples would have a varied composition. Therefore syngas yield from the different sample sizes would not be representative of the overall syngas potential of the harvested vine. Thus, the vines were all milled to produce uniform powdered samples, which were stored in airtight bags.

3.2 Biomass Analysis

Collected samples were also sent to HRL Technology to measure the total moisture content of the samples, ash content at 550°C, volatile matter, fixed carbon, carbon, hydrogen and nitrogen content, and the total sulphur [48].

3.2.1 Moisture Content

The total moisture was measured according to the CEN/TS 15414:2010 standard [49].

The samples were prepared according to I.S. EN 1413:2011 to produce a test sample with a particle size of ≤1 mm. An empty weighing dish and lid were dried at 105 ± 2°C until constant mass was reached before allowing it to cool to room temperature in a desiccator. The weighing dish and lid was then weighed to the nearest 0.1 mg. A minimum of 1 g of the sample was then added to the weighing dish in an even layer and it was reweighed to the nearest 0.1 mg. The uncovered weighing dish with the sample inside, and the lid was then heated to 105 ± 2°C until constant mass was reached under a nitrogen atmosphere to avoid oxidation of the material. Once constant weight was reached, the lid was placed on the weighing dish in the oven. The dish and contents were transferred to the desiccator and allowed to cool to room temperature. The dish, sample and lid was then weighed to the nearest 0.1 mg rapidly after reaching room temperature [49].

The moisture content, M_{ad}, expressed as mass fraction in percent, was then calculated using Formula 20:

$$M_{ad} = \frac{m_2 - m_3}{m_2 - m_1} \times 100 \tag{20}$$

where m_1 is the mass of the empty weighing dish and lid, m_2 is the mass of the weighing dish, lid and sample before drying, and m_3 is the mass of the weighing dish, lid and sample after drying [49].

3.2.2 Ash Yield at 550°C

The ash yield at 550°C was measured according to the I.S. EN 15403:2011 standard [50].

An inert dish was heated in a furnace to 550 ± 10°C for at least 60 min. It was then cooled to room temperature in a desiccator and weighed to the nearest 0.1 mg. Approximately 1 g of the analysis sample was spread across the bottom of the dish and weighed to the nearest 0.1 mg. The loaded dish was then placed in the cold furnace. The temperature was then raised at 5°C per minute to 250 ± 10°C over a period of 50 minutes. This temperature was maintained for 60 minutes to allow the volatile materials to leave the sample before ignition. The furnace was then heated once more at 5°C per minute to 550 ± 10°C over a period of 60 minutes. Once the furnace had reached 550°C, the furnace was kept at this temperature for at least 120 minutes [50].

The dish and contents were removed from the furnace and cooled on a thick metal plate for 5 to 10 minutes before being transferred to a desiccator without desiccant to allow to cool to ambient temperature. As soon as ambient temperature was reached, the ash and dish was weighed to the nearest 0.1 mg [50].

The ash content on dry basis, A_{db}, expressed as mass fraction in percent, was then calculated using Formula 21:

$$A_{db} = \frac{m_3 - m_1}{m_2 - m_1} \cdot 100 \cdot \frac{100}{100 - M_{ad}} \tag{21}$$

where m_1 is the mass of the empty dish, m_2 is the mass of the dish and sample, m_3 is the mass of the dish and ash, and M_{ad} is the moisture content of the sample, in percent [50].

3.2.3 Volatile Matter and Fixed Carbon

The volatile matter and fixed carbon was measured according to the I.S. EN 15402:2011 standard [51].

A crucible with lid was placed in a furnace and a temperature of 900 ± 10°C was maintained for 7 minutes. The crucible was then allowed to cool to room temperature on a thick metal plate. As soon as the crucible had cooled, it was weighed to the nearest 0.1 mg. 1 – 2 ± 0.1 g of undried sample was then weighed into the crucible, to the nearest 0.1 mg, and the crucible, with its lid on, was tapped on a clean surface until the sample formed an even layer on the bottom of the crucible [51].

The crucible was then transferred to the hot furnace and left 420 ± 5 seconds before being removed and cooled to room temperature. Once cool, the crucible was weighed to the nearest 0.1 mg in the same manner as for the empty crucible [51].

The volatile matter, $V_{ad,db}$, in the analysed sample, in dry basis, expressed as mass fraction in percent, is given by Formula 22:

$$V_{ad,db} = 100 \cdot \left[\frac{(m_2 - m_3)}{(m_2 - m_1)} - M_{ad} \right] \cdot \frac{100}{(100 - M_a)} \tag{22}$$

where m_1 is the mass of the empty crucible and lid, m_2 is the mass of the crucible, lid and

sample before heating, m_3 is the mass of the crucible, lid and sample after heating, and M_{ad} is the moisture content of the sample, in percent [51].

The volatile matter and fixed carbon make up the total organic matter of the biomass. Fixed carbon is the relative part of carbon contained in the biomass that can only be remove in high temperature environments with oxygen present. The fixed carbon in the sample, expressed as mass fraction in percent is given by Formula 23 [51]:

$$\text{fixed carbon} = 100 - \text{moisture content} - \text{volatile matter} - \text{ash} \tag{23}$$

3.2.4 Carbon, Hydrogen, Nitrogen and Sulphur

The carbon, hydrogen and nitrogen content of the biomass samples was determined according to the I.S. EN 15407:2011 standard [52]. The sulphur content was measure according to the I.S. EN 15408:2011 standard [53].

Test portions of the samples were weighed and placed into the instrumental apparatus used for the analysis, and appropriate cycles for the instrument were used for each test. The results were given directly from the instrument [52], [53].

3.2.5 Oxygen Content

The oxygen content of the biomass samples was determined according to the ASTM 870-82 standard [54].

The carbon, hydrogen, sulphur, nitrogen and oxygen make up the total organic matter of the biomass. The oxygen in the sample, expressed as mass fraction in percent is given by Formula 24 [54]:

$$O = 100 - (C + H + S + N + A_{db}) \tag{24}$$

where O is the oxygen content of the sample, C is the carbon content of the sample, H is the hydrogen content of the sample, S is the sulphur content of the sample, N is the nitrogen content of the sample, and A_{db} is the ash content of the sample, in percent [54].

3.3 Thermodynamic Analysis

AspenTech's Aspen Plus® simulation software was used to model the theoretical syngas yield from the gasification of the tomato vine [55]. The system was modelled in a RGIBBS reactor using Gibbs free energy minimisation in order to calculate the syngas yield under varied conditions. Dry and steam gasification were modelled with biomass-to-oxidiser ratios of 1:1, 1:2 and 1:3 for each of the three sample compositions of the collected vine.

In the model, the samples were heated to 450°C under an inert atmosphere before the oxidising gas was fed into the reactor and heating continued to 900°C, where it was held isothermally for 20 minutes. Typical products of gasification reactions were used, namely CO_2, CH_4, CO, H_2O, H_2 and O_2. H_2 and CO yields and molar fractions in the product gases were calculated for each of the scenarios. Additionally, a sensitivity analysis was performed to determine the

effect of temperature on the decomposition of the biomass at temperatures between 300°C and 900°C without an oxidising agent present.

3.4 Thermogravimetric Analysis

Dry gasification was undertaken within a benchtop thermogravimetric analysis (TGA) apparatus (NETZCH STA 449 F3) for all samples, using a differential thermal analysis (DTA) sample carrier. The reactor was heated under argon (Ar) flow of 125 ml min^{-1} to 900°C at a rate of 20°C min^{-1}. When it had reached 450°C, 10 ml min^{-1} of CO_2 was fed into the reactor, and the Ar flow rate was reduced to 115 ml min^{-1}. The sample was then held at 900°C for 20 minutes before being cooled to ambient temperature at 20°C min^{-1}, with the CO_2 flow being shut off at 450°C. The thermogravimetry (TG) was recorded continuously during gasification for each of the samples.

Pyrolysis was also undertaken in the TGA under an Ar environment in order to obtain a relation between the temperature and the thermal decomposition of the tomato vine. Heating rates of 5, 10 and 20°C min^{-1} were used in order to ensure that the kinetics of the reaction did not limit the accuracy of the results.

3.5 Dry and Steam Gasification

Gasification was performed in a vertical down-flow tube reactor centred in an electric IR gold image furnace (P4C-VHT, Advance Riko). Precisely 1 g of the powdered vine was placed between two porous aluminosilicate mats within an alumina reactor tube (99.98% Al_2O_3). The mats acted as a sample stage and upper protective layer for the powdered vines to ensure that the sample remained within the heating zone of the furnace during gasification. Samples of this size were chosen in order to limit the possibility of an accumulation of tars produced during gasification from accumulating in the gas lines and interfering with the operation of the reactor. A gap of approximately 20 mm was maintained between the vine sample and the upper alumina mat in order to facilitate solid-gas mass transfer. In order to maintain uniform heating throughout the sample bed it was placed in the middle of the furnace heating zone, with a B-type thermocouple sealed in an alumina sheath placed directly beneath the sample stage to regulate and record the temperature during gasification.

The reactor tube was placed in the gas line with Swagelock fittings, and the concentration of the product gases was recorded using a quadrupole mass spectrometer (OmniStar™GSD 320, Pfeiffer Vacuum) every 0.9 seconds, approximately. Inlet gas mixtures were regulated using flow rate controllers (F201CV, Bronkhorst) and actuated valves (1315R, Swagelok), operated by the LabVIEW (National Instruments) software program. A schematic of the reactor tube set-up is shown below in Figure 3.

The system was purged with Ar (COREGAS grade 5.0) at a flow rate of 500 ml min^{-1} to eliminate any gas species from the reactor and gas lines at ambient temperature. Once purged, the furnace was heated at a rate of 100°C min^{-1} to 900°C, where it was held isothermally for 40 minutes before cooling to ambient.

For dry gasification, CO_2 was used as the oxidising gas, with 5, 10, 15, and 20 ml min^{-1} of CO_2 (COREGAS grade 4.5) fed into the reactor tube when the furnace temperature was over

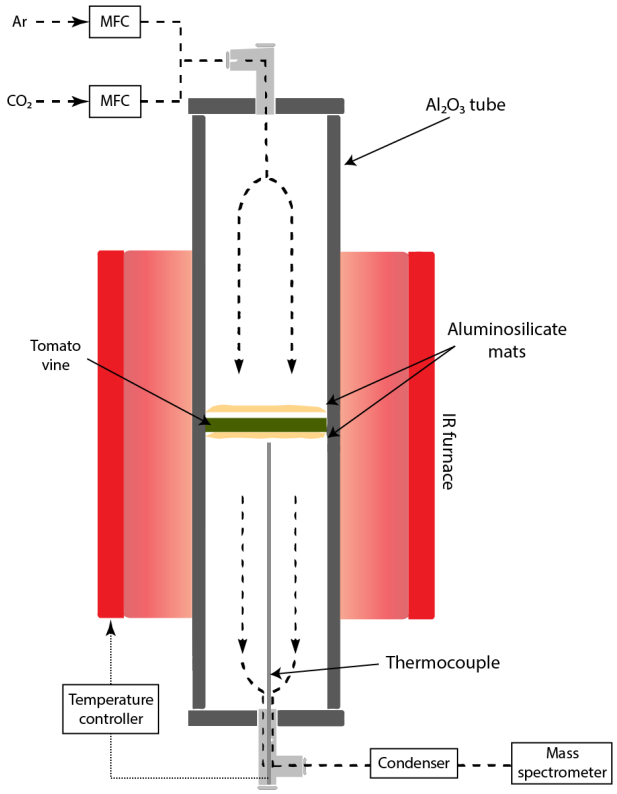

Figure 3: Schematic of the tube reactor for IR furnace gasification. MFC: mass flow controller.

400°C during both heating and cooling. Below this temperature, only inert Ar was present in the inlet gas feed. During heating and gasification, the total gas flow through the reactor was 200 ml min^{-1}, with Ar acting as a carrier species and making up the balance from the oxidiser gas volumes.

During steam gasification, steam was generated from a deionised (DI) water bubbler at 95°C. When the furnace temperature was above 400°C, Ar was passed through the bubbler at 10, 15, and 20 ml min^{-1} to feed steam into the reactor at the various flow rates. A total of 200 ml min^{-1} of Ar was fed into the reactor, with the difference bypassing the bubbler as normal.

3.6 Post-Gasification Residue

Post-gasification residue was separated from the sample stage after gasification and weighed before being stored in airtight containers. The amount and appearance of the remaining material was recorded, however, the volume of residue was less than necessary to undertake chemical testing, and so further analysis of the material was not possible.

3.7 Harvest Potential Calculations

The mass of the product gases that could be obtained from gasification of one tonne of tomato vine was calculated using Formula 25:

$$m_{\text{gas}} = \frac{m_{\text{gas,exp}}}{m_{\text{sample}}} \cdot 1\,000 \tag{25}$$

where m_{gas} is the total mass of gas produced with gasification of one tonne of tomato vines, $m_{\text{gas,exp}}$ is the mass of gas produced during the gasification experiment, and m_{sample} is the mass of tomato vine sample used during gasification.

4 Results and Discussion

4.1 Biomass Analysis

The results of the biomass analysis undertaken by HRL Technology are displayed below in Table 1, with the oxygen calculated by difference included.

As can be seen in Table 1, the moisture content of the vines is not constant across samples. Whilst each of the values lies within 10% of their mean, the variation between the three samples shows the drying requirements for vines collected across a region could vary greatly depending on factors such as weather conditions, tomato variety and time between fruit and vine harvest.

The ash content of the vines is relatively high compared to other forms of biomass such as woods and nut shells, although they are similar to other crops waste materials such as wheat straw, sugarcane bagasse and olive refuse, which is consistent with results in literature [56]. Additionally, there is a considerable variation in the ash content of Sample 1 compared to Samples 2 and 3, which may be due to varied inorganic contents in the soil across the growing region. Practically, this would mean that a gasification system would have to be optimised for the maximum ash content across all vine samples in the harvest area to ensure that operational complications from ash deposition did not occur.

The volatile matter of the samples is lower than that of wood-type biomass, but is in the typical range for agricultural wastes such as wheat straw and lucerne stalks [56]. The fixed carbon is slightly lower than is typical but this is expected when taking the higher ash content of the samples into account.

Table 1 also shows significant variance in the composition of the samples supplied. This indicates that sourcing material from different growing locations within a region may cause variations in the amount and composition of syngas produced. This would need to be monitored during operation of a commercial plant to ensure that the desired syngas composition is obtained.

Table 1: Results of biomass analysis

	Sample 1	**Sample 2**	**Sample 3**
Moisture ($\%_{ar}$)	17.7	19.3	16.3
Ash yield ($\%_{db}$)	16.8	10.6	10.8
Volatile matter ($\%_{db}$)	68.6	72.4	72.8
Fixed carbon ($\%_{db}$)	14.6	17.0	16.4
Carbon ($\%_{db}$)	36.0	39.9	40.9
Hydrogen ($\%_{db}$)	5.2	5.4	5.6
Nitrogen ($\%_{db}$)	1.53	1.08	2.05
Sulphur ($\%_{db}$)	0.36	0.25	0.20
Oxygen ($\%_{db}$)	40.11	42.77	40.45

For commercial operation, sulphur levels in the samples is of particular note. Sulphur is especially aggressive to reactor materials and catalysts, and poses human health concerns when present as sulphur dioxide, which is produced during gasification. The sulphur levels in the obtained samples are very low when compared to coal used in gasification, but are significantly higher than other biomass types, which is not unexpected for an agricultural waste [56]. With this level of sulphur in the samples, gas scrubbing would be necessary in a commercial plant to ensure that it did not damage the reactor or pose health risks.

4.2 Thermodynamic Analysis

The H_2 and CO yields were calculated for gasification of 1 kg of each of the three tomato vine samples and are shown below in Figure 4 below.

As can be seen in Figure 4, H_2 yields are significantly higher when steam gasification is performed, with higher amounts of H_2 being obtained with higher steam-to-biomass ratios. This trend is inverted when dry gasification is performed, with the highest H_2 yield obtained with the 1:1 CO_2-to-biomass ratio. Likewise, the maximum yield of CO is obtained with high levels of excess CO_2 during dry gasification, and the minimum obtained with excess H_2O during steam gasification. This would indicate that the WGS and the RWGS reactions are occurring with excess amounts of H_2O and CO_2, respectively.

Whilst excess oxidiser improves the thermodynamics of the reaction to shift the equilibrium toward the desired products, the above simulation shows that significantly changes the yield and composition of the syngas due to the WGS and RWGS for steam and dry gasification, respectively. Controlling the temperature of the reactor during gasification could limit the activity of this reaction as the WGS products are favourable at lower temperatures. The increased energy requirement from the use of excess oxidisers due to the latent heat of water and separation requirements must also be taken into account when considering the biomass-to-oxidiser ratios.

Additional to the yield of syngas achieved during the simulation, the H_2/CO molar fractions in the product gases was obtained. These results for Sample 2 are shown below in Figure 5, and in Figure 18 of Appendix A for Samples 1 and 3.

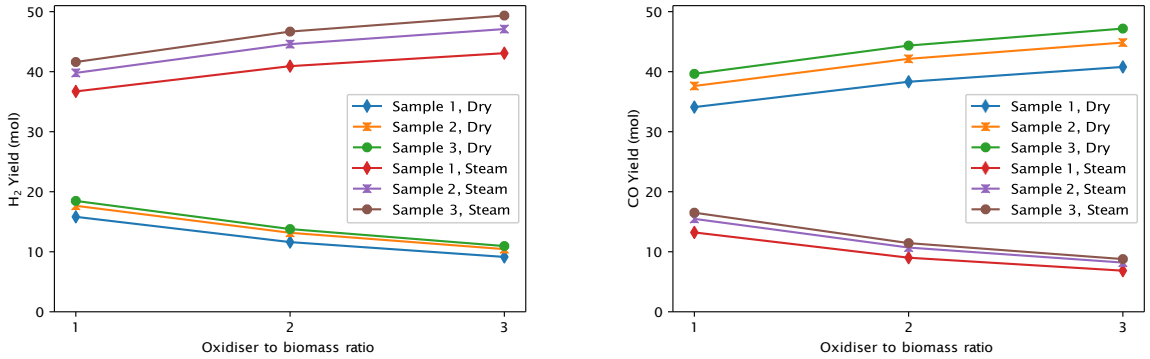

(a) H_2 yield (b) CO yield

Figure 4: Syngas yields simulated in Aspen Plus® for gasification of 1 kg of tomato vine

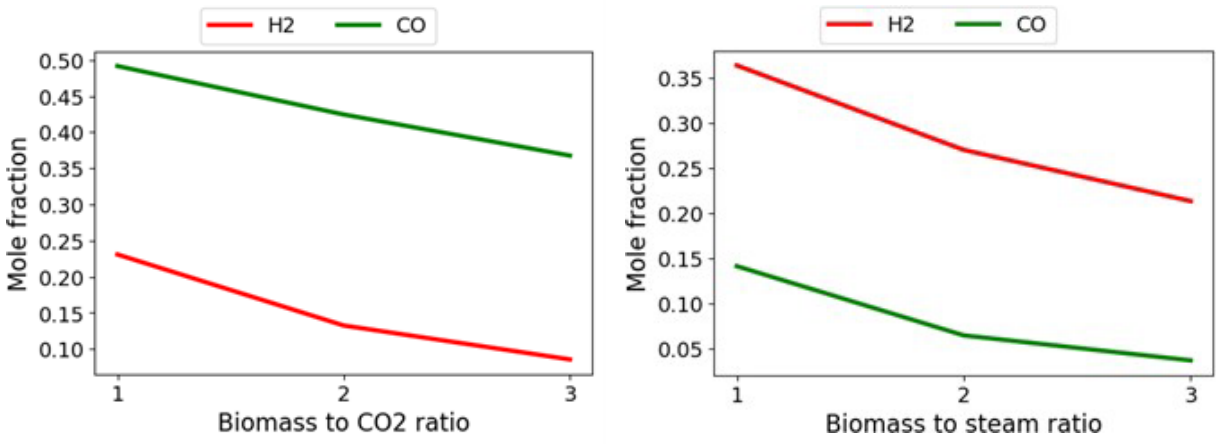

(a) Sample 2, dry gasification (b) Sample 2, steam gasification

Figure 5: Molar fractions of H_2 and CO in the produced syngas for Sample 2

Once again, it is clear that increasing the amount of CO_2 and H_2O oxidiser decreases the molar fraction of H_2 and CO during dry and steam reforming, respectively. However, the similar downward trend in the other syngas product is due to the increased mole fraction of the oxidiser gas still present in the sample after complete conversion of the biomass has occurred, causing the syngas to have a smaller total percentage of the product gases. This pushes the thermodynamic equilibrium toward the syngas products and would help to achieve complete conversion of the biomass materials, although will impact the composition of the syngas due to the WGS reaction as seen above.

The results of the sensitivity analysis to determine the effect of temperature on the product gases is shown below in Figure 6.

Figure 6 shows that syngas production is favourable above 600°C, with little H_2 being produced below this temperature. syngas production improves significantly between 600°C and 800°C, but above this temperature there is no significant increase in the mole fraction of H_2 and CO. Whilst the equilibrium composition is not largely affected by increase of temperature between 800°C and 900°C, in practice the kinetics of the reaction may be the limiting

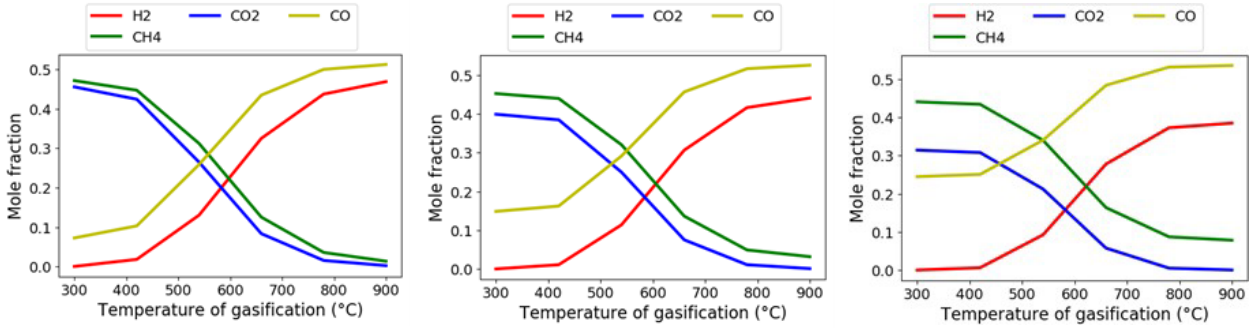

(a) Sample 1 (b) Sample 2 (c) Sample 3

Figure 6: Molar fractions of product gases for gasification of tomato vine without oxisider simulated between 300°C and 900°C

factor during gasification and so higher temperatures would increase the likelihood that the equilibrium composition to be reached.

Complete conversion of methane and CO_2 is approximately achieved at 900°C for Samples 1 and 2, but relatively large amounts of methane is still present in the product gases at high temperatures for Sample 3. This would be due to the relatively high proportion of carbon that is present in Sample 3 compared to oxygen. Methane reforming of this remaining methane would occur during gasification with an oxidiser present in practice.

4.3 Thermogravimetric Analysis

The TG recorded during dry gasification is shown for each of the samples below in Figure 7. The period where the furnace is between 50°C and 150°C is highlighted in blue, which indicates the area where the moisture content in the vines is evaporated. The area between 200°C and the start of the CO_2 flow is shaded grey and shows the weight loss during pyrolysis of the vine where it is decomposing in the inert atmosphere.

Figure 7 shows the moisture content in the vines is between 5 and 8% of the initial mass.

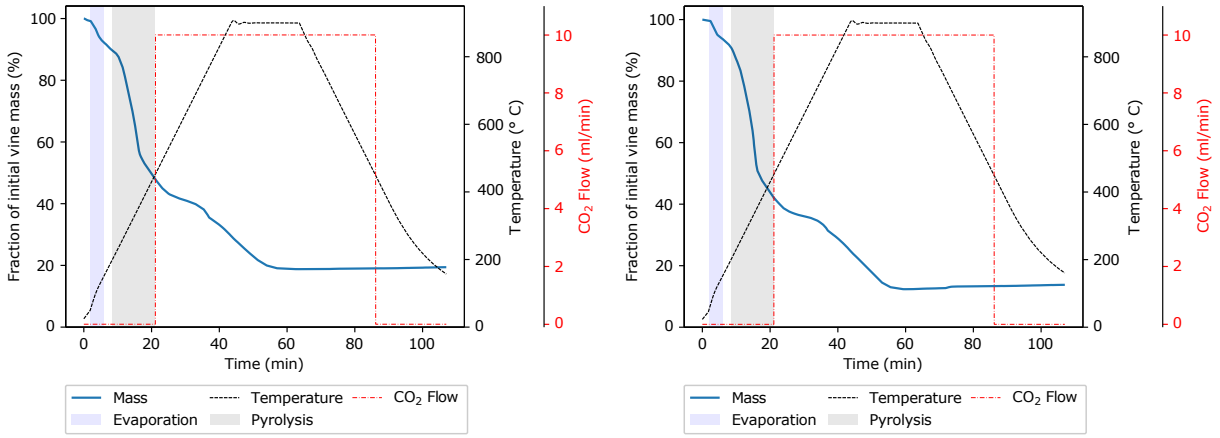

(a) Sample 1

(b) Sample 2

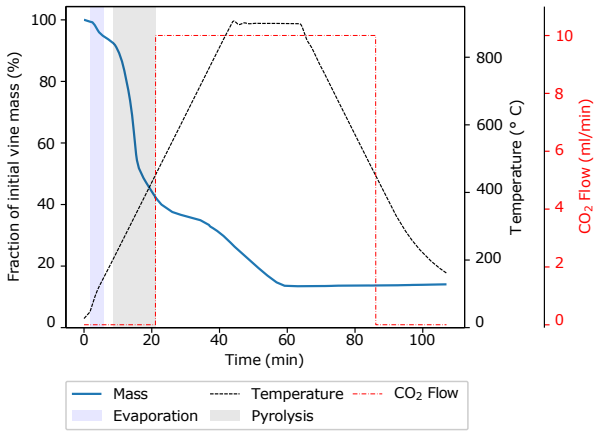

(c) Sample 3

Figure 7: Thermogravimetry of the samples during dry gasification

Whilst the vines were dried and stored in airtight packages before use in the experiments, the hydrophilic nature of the biomass means that some of this moisture content would have been reabsorbed during the grinding and handling of the samples. Additionally, to prevent any decomposition of the vines during the initial drying procedure, a lower drying temperature was used and therefore some fraction of the inherent moisture in the sample may not have been removed during the drying process. The relatively large variation between the samples is due to any discrepancies in the time taken to grind the samples, as well as the differences in the composition of the biomass of each sample.

A large decrease in the mass of the samples occurs between 200°C and the start of the CO_2 flow through the reactor, averaging 47% of the total mass of the samples. This indicates that a large amount of the biomass decomposes through pyrolysis before gasification begins when this heating rate is used. The total mass lost during gasification ranges between 71% and 86%, with an average of 84% across the three samples. This shows that full oxidation of the fixed carbon does not occur during this gasification regime. This is partly due to mass transport limitations that the reaction would undergo in the TGA apparatus, as gas-solid phase is limited by the flow into the crucible.

The mass is observed to minimise at around 19, 12 and 13 minutes into the experiment for Samples 1, 2 and 3, respectively, before slightly increasing during the remainder of the experiment. This is likely due to coke formation occurring in the reactor when the absence of other gases from the decomposition of the vine increases the molar fraction of CO_2 in the reactor and increases the thermodynamic favourability of carbon deposition. The amount deposited is relatively small but this should be taken into account in the reactor design to limit the amount of carbon deposited. This could be done by decreasing the time on stream after the vine has been gasified fully and decreasing the molar fraction of the CO_2 in the carrier gas.

The mass loss during pyrolysis for each of the samples is shown below in Figure 8, with the time period where evaporation takes place highlighted.

As seen in Figure 8, there a significant mass loss due to evaporation of moisture during heating, with the loss from each sample being consistent with that observed during the gasification reactions. Similar overall mass loss is observed across samples, with a higher percentage of the total mass remaining at the end of the sample due to the lack of oxidiser meaning that the fixed carbon remains in the sample. The slight difference in the mass remaining across the samples is consistent with the results of the analysis performed by HRL.

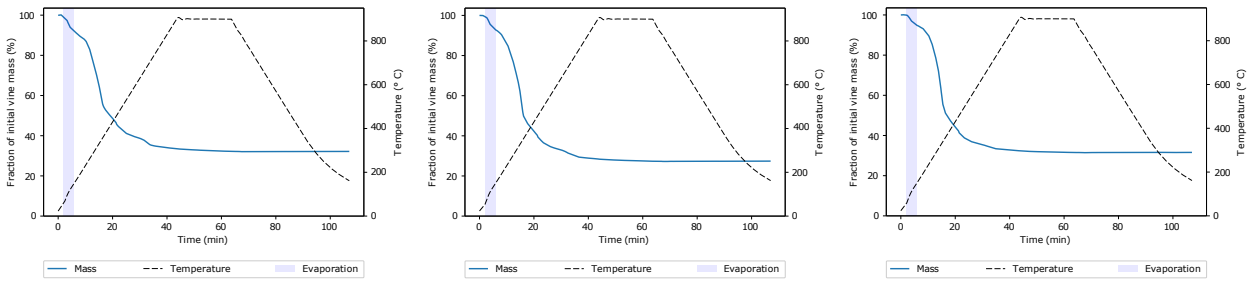

(a) Sample 1 (b) Sample 2 (c) Sample 3

Figure 8: Thermogravimetry of the samples during pyrolysis

The results of the sensitivity analysis determining the effect of the furnace heating rate on the pyrolysis are shown below in Figure 9. Once again the range between 50°C and 150°C is highlighted to show the mass low due to the evaporation of all moisture.

Moisture loss of about 10% of the initial mass of the vines is seen across the experiments. This is slightly higher than the results seen above, and is likely due to the smaller amount of vine that was used during these experiments, which would improve the mass transport through the sample carrier. Higher moisture loss below 150°C is seen with the slower heating rates, which indicates the kinetics of evaporation may be a limitation of drying in the other experiments.

However, the overall mass loss observed between the samples has the inverse trend, with the total mass removed being the highest for the experiment with the heating rate of 20°C min^{-1}. This shows that the kinetics of the pyrolysis reaction are not limiting the decomposition of the reaction. The proportion of the sample left with slower heating rates may be due to structural changes in the molecular structure of the biomass at lower temperatures increasing the amount of fixed carbon in the sample, as carbon formation is more favourable at lower temperatures.

4.4 Dry and Steam Gasification

4.4.1 Volumetric Flow Rates During Gasification

The volumetric flow rates of the product gases recorded during dry gasification of Sample 2 are shown below in Figure 10. The same data is shown in Figures 19 and 20 of Appendix B for Samples 1 and 3, respectively.

Figure 10 above shows a large spike in the CO_2 flow as the oxidiser starts to flow through the reactor at 400°C. This spike quickly tapers off as the temperature rises and thermodynamic favours the syngas products. A similar spike in the methane production is seen during the initial moments of the experiment as the furnace is hot enough for the vine to break down but not yet hot enough for methane reforming to occur. CO production starts at around 500°C when the CO_2 would begin oxidising the carbon present in the sample. Production then continues to grow as the methane reforms, with the peak production in all experiments

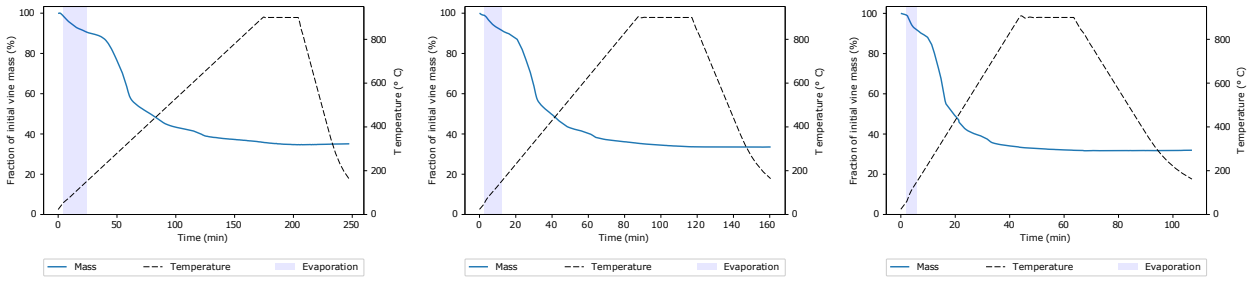

(a) 5°C min^{-1} (b) 10°C min^{-1} (c) 20°C min^{-1}

Figure 9: Thermogravimetry of Sample 1 during pyrolysis with varied heating rates

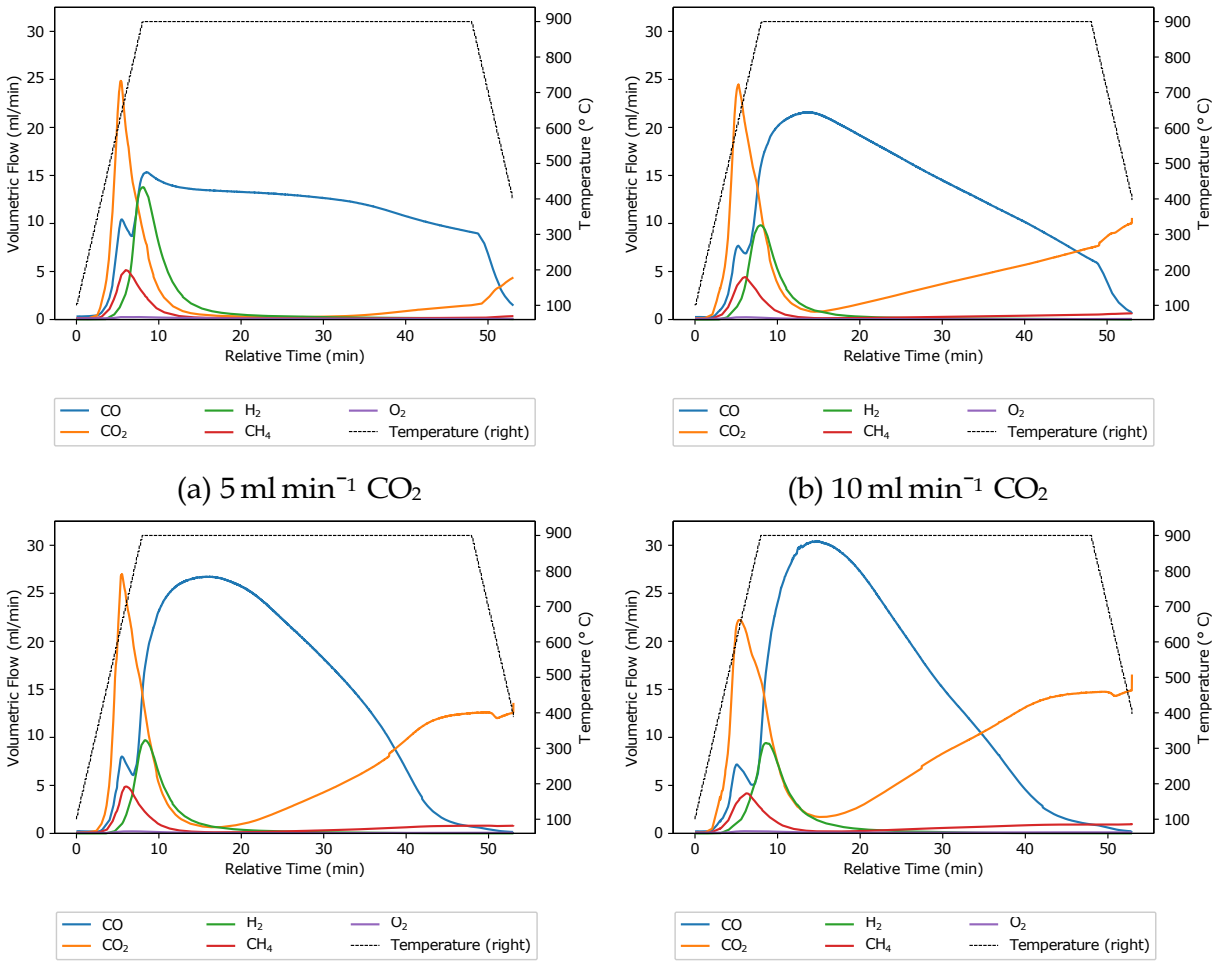

(a) 5 ml min^{-1} CO_2

(b) 10 ml min^{-1} CO_2

(c) 15 ml min^{-1} CO_2

(d) 20 ml min^{-1} CO_2

Figure 10: Flow rates of product gases recorded during dry gasification of Sample 2

occurring approximately at the same time as the furnace temperature peaks. H_2 peaks just before this time as the volatile matter in the sample is used up and methane is no longer produced and reformed. CO remains high after the other products are no longer present in the product gases as all remaining fixed carbon is oxidised and any H_2 produced undergoes the RWGS to be converted into CO_2 and H_2O.

In Figure 10a and 10b, CO production drops off sharply during cooling, at around 700°C, indicating that full oxidation of the fixed carbon had not occurred due to insufficient oxidiser being present during gasification. This aligned with the state of the ash present in the reactor after gasification, which contained relatively large amounts of black residue compared to those when higher CO_2 flow rates had been used, which were largely pale grey in appearance. In Figures 10c and 10d, CO production tapers off more steadily whilst the furnace is still at 900°C, coinciding with increased flow of CO_2. This shows that full oxidation of the fixed carbon in the samples is achieved during gasification with the higher oxidiser flow rates.

The volumetric flow rates of the products during steam gasification for Sample 2 are shown below in Figure 11. The results for Samples 1 and 3 are shown in Figures 21 and 22 of Appendix B, respectively.

Similar to dry gasification, Figure 11 shows a spike of CO_2 production during the heating of the furnace. However, as no CO_2 is being fed into the reactor, this spike is attributed to the decomposition of the tomato vine during heating. A smaller peak of methane starts shortly after the increase in CO_2 production due to insufficient reactor temperatures to convert these products to syngas. The sharp decline in CO_2 and methane production as the temperature in the furnace reaches around 750°C shows the start of mixed methane reforming to produce syngas.

The production of H_2 and CO during the heating regime of the furnace whilst methane reforming is not occurring results from the oxidation of the carbon in the sample by the H_2O, as well as breakdown of simpler biomass molecules directly to syngas upon heating. In all experiments there is a drop in the H_2 and CO production after the initial spikes from the vine decomposition and methane reforming, before it once again increases, with this occurring earlier with higher rates of oxidiser flow. This drop in syngas production may be due to large amounts of the volatile matter contained in the samples already having decomposed and so little gaseous products are produced whilst the longer biomass molecules are breaking down in the solid phase of the sample.

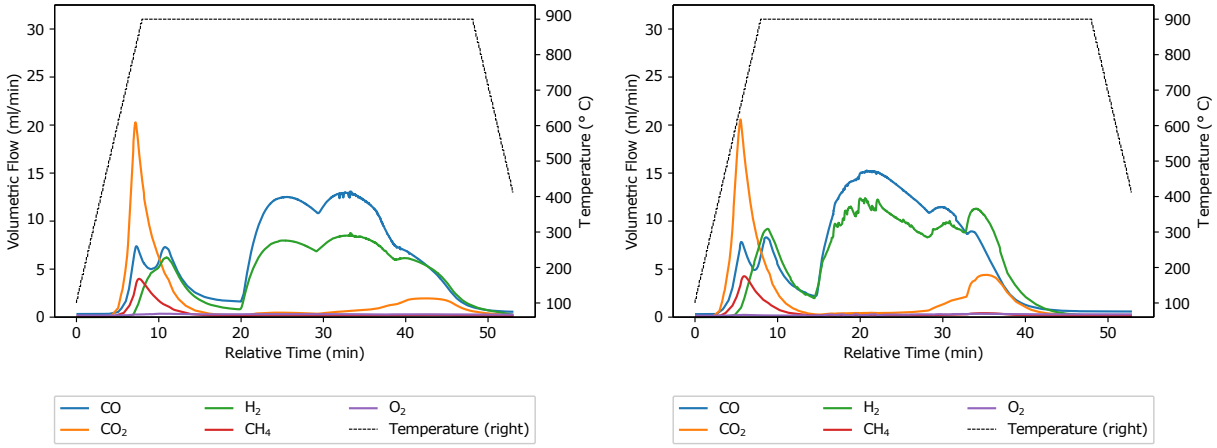

(a) 10 ml min^{-1} argon through bubbler

(b) 15 ml min^{-1} argon through bubbler

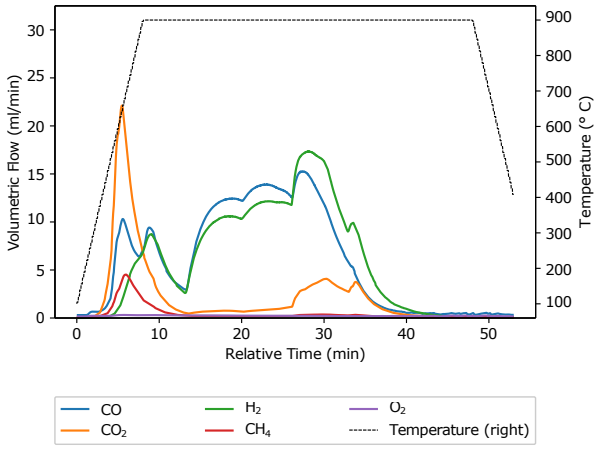

(c) 20 ml min^{-1} argon through bubbler

Figure 11: Flow rates of product gases recorded during steam gasification of Sample 2

The syngas production tapers off when the furnace is still at 900°C for all samples, indicating that the oxidiser flow rate is sufficient to oxidise all fixed carbon in the sample. However, this is not the case for Samples 1 and 3, which show a drop off in the production of CO when the furnace cools. This discrepancy between samples may be caused by the increased ash content in Sample 1 prohibiting mass transfer in the sample, and the lower proportion of oxygen relative to carbon in Sample 3, meaning more H_2O is required to oxidise the carbon in the sample.

The production of CO_2 in the latter stages of the experiment, coinciding with a decrease in CO and increase in H_2 shows that the WGS reaction is occurring after the volatile matter in the sample has been converted and the molar fraction of H_2O in the reactor increases, pushes the equilibrium composition towards H_2 and CO_2.

4.4.2 Experimental Gas Yields

The H_2 and CO yields obtained during gasification are shown below in Figure 12.

Figure 12a shows an approximate upwards trend in the volume of H_2 with oxidiser flow during steam gasification. Sample 2 produces considerably higher amount of H_2 compared to the other two samples, which is due to the low amounts of ash content and higher proportion of carbon in this sample, which increases the volume of H_2O that can be reduced. Sample 1 shows the lowest amount of H_2 produced, which is consistent with the higher ash content measured during proximate analysis.

During dry gasification, the highest volume of H_2 produced is with 5 ml min^{-1} CO_2, which is consistent with the thermodynamic modelling and indicates that the RWGS reaction is occurring in the reactor with the excess CO_2. This trend stabilises for all samples with 10 and 15 ml min^{-1} CO_2, which indicates the faster gasification of the sample due to the higher oxidiser flow rate decreases the favourability of the RWGS as the molar fraction of the CO_2 in the reactor is lower during the period where H_2 is also present. The increase in the amount of H_2 produced with the highest flow rate for Sample 3 may be caused by the

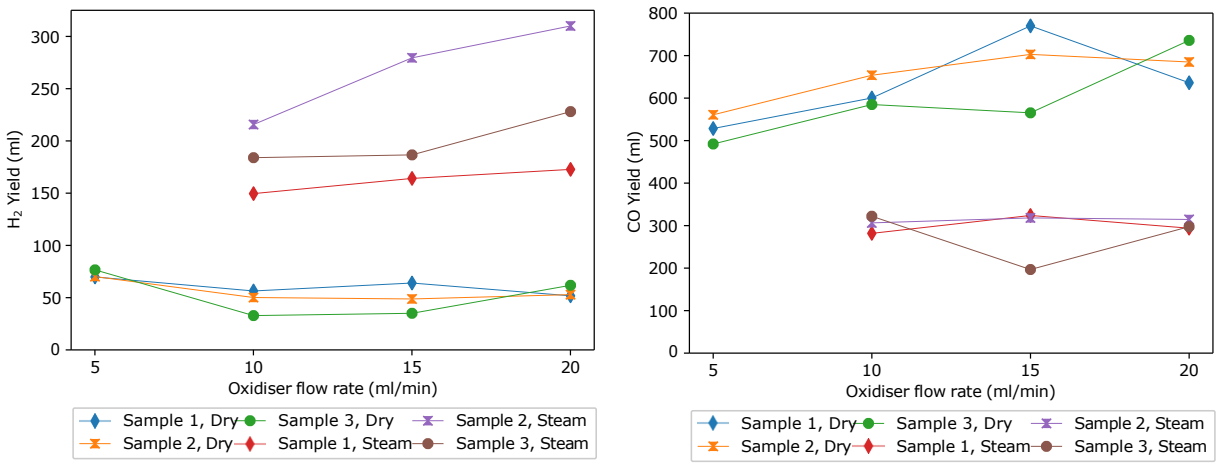

(a) H_2 yield

(b) CO yield

Figure 12: H_2 and CO yield during both dry and steam gasification

relatively low proportion of oxygen in this sample compared to carbon, which increases the volume of oxidiser required to gasify the entire sample and liberate all hydrogen from the vine. This is confirmed when examining the gas flow rates during the experiment, where the CO production falls off quickly as the furnace cools for all experiments except that with 20 ml min^{-1} CO_2, showing that complete oxidation of the biomass is not reached for these experimental regimes.

Figure 12b shows a nearly constant production of CO during steam gasification, with Sample 3 15 ml min^{-1} CO_2 being an outlier in this. This indicates that the increased oxidation of the samples due to the higher oxidiser flow makes up for the CO that is converted in the WGS reaction. Additionally, as the WGS shift is favourable at lower temperatures, the amount of CO likely to be converted is relatively small. The outlier in Sample 3 may be due to insufficient oxidation of the sample while the WGS reaction is still occurring.

There is a general upward trend, with outliers once again at 15 ml min^{-1} CO_2 for both Samples 1 and 3. This trend shows that the increased CO_2 flow increases the fraction of the vine that is gasified. Across the three samples, there is little to no increase in the CO yield between the two highest oxidiser flow rates. This may be because full oxidation is achieved at 15 ml min^{-1} of CO_2 and the faster gasification of the vine causes the molar fraction of CO_2 to be lower when H_2 is present in the reactor and therefore the RWGS reaction is less favourable. Additionally, the higher molar fraction of CO_2 may cause coking within the reactor and so the CO yield is lowered. The reasons for the two outliers in this data are not clear although it may be due to the varies composition of the samples causing different molar fractions of the reactants and products in the furnace and therefore yielding different quantities of the gases.

The total H_2 and CO yields including the syngas obtained from reforming the methane produced during gasification is shown below in Figure 13, with complete conversion assumed to determine a theoretical maximum of syngas production from the methane.

The overall yield of syngas is increased significantly when the methane present in the product

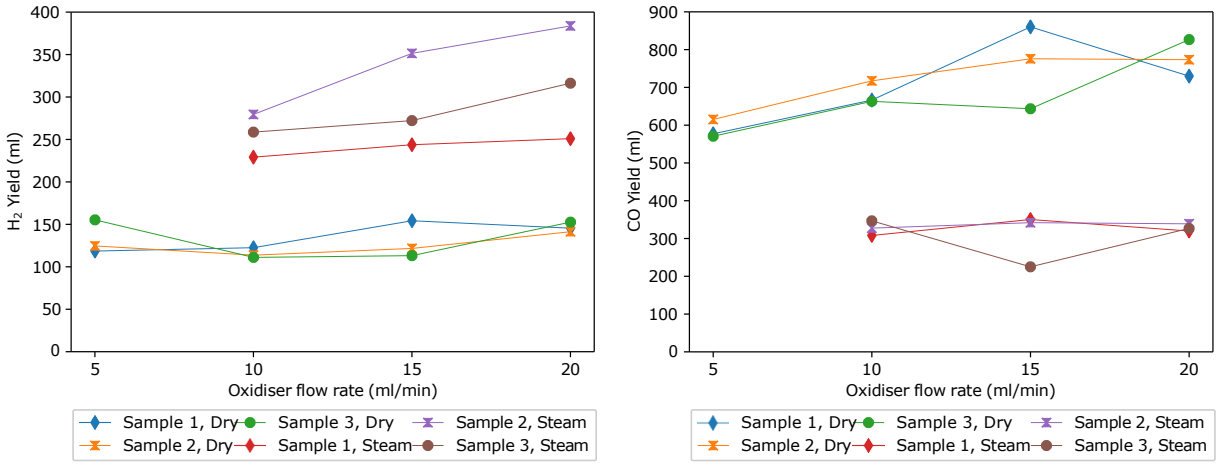

(a) H_2 yield

(b) CO yield

Figure 13: H_2 and CO yield during dry and steam gasification with complete conversion of methane produced during gasification

gases is reformed, with roughly the same proportions between the regimes. This shows the importance of reactor design in ensuring that the products of gasification has sufficient residence time in a reactor at reforming temperatures in order to obtain the maximum syngas yield. In the reactor setup used, the majority of the methane that is present in the product gases is released before the temperature of the unit reaches 900°C, implying that in practice vines should be fed into an isothermal furnace rather than in a batch reactor, or a secondary reforming chamber is needed.

The H_2/CO yield ratio was calculated for the each of the experiments, and when assuming complete conversion of the produced methane with dry and steam reforming for the respective gasification modes. These results are shown below in Figure 14.

Figure 14 show low H_2/CO ratios for all samples undergoing dry gasification. Experiments with 5 ml min^{-1} of CO_2 have the highest ratio, which is in agreement with the above results showing that full gasification of the fixed carbon and the RWGS is more likely in the experiments with higher CO_2 flow. The plateau of the ratio for the other experimental regimes indicates that the differences seen in the yields in Figure 12 are more likely due to increased conversion of all biomass in the sample rather than higher rates of the RWGS occurring with higher CO_2 flow.

For steam gasification, Sample 2 shows an upward trend in the H_2/CO ratio with oxidiser flow rate. The outliers seen in the results of the H_2 and CO yields are seen again here, with the low production of CO during gasificaiton of Sample 3 with 15 ml min^{-1} of Ar through the water bubbler giving a high H_2/CO ratio for that experiment.

4.5 Post-Gasification Residue

The amount of post-gasification residue collected was modest for all experiments, and separation of the aluminosilicate mat from the ash/biochar was difficult. The colour of the biochar ranged from pale grey to black, with the samples gasified with higher oxidiser flow rates being lighter in colour. Visual evidence of carbon was apparent in samples with 5

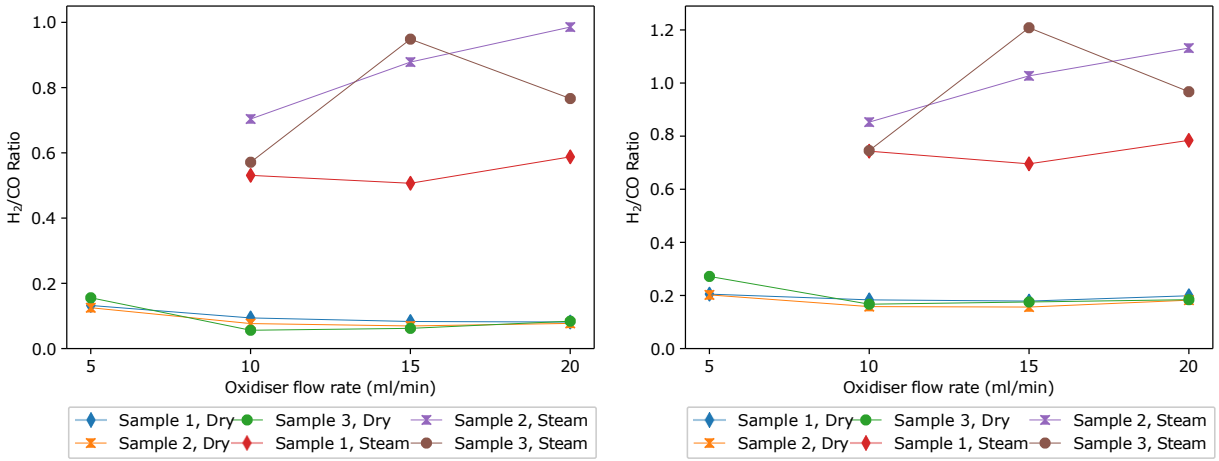

(a) Without methane reforming

(b) With methane reforming

Figure 14: H_2:CO yield ratios

and 10 ml min^{-1}, with the centre of the sample being darker in colour than the extremities, whereas the samples with 15 and 20 ml min^{-1} were mostly ash-like in colour and consistency. The residue was darker in the centre of the sample for many of the samples, indicating that mass-transfer limitations in the sample bed limited complete gasification of the sample. This indicates that reactor design may be limited to those that feature high mass-transport, and the biochar that is produced would depend heavily on the reactor design and it is therefore futile to analyse the properties of the biochar obtained from the reactor configuration used to obtain these results.

4.6 Harvest Potentials

4.6.1 Gas Masses

The mass of the H_2, CO and methane produced during gasification of one tonne vine are shown below in Figure 15.

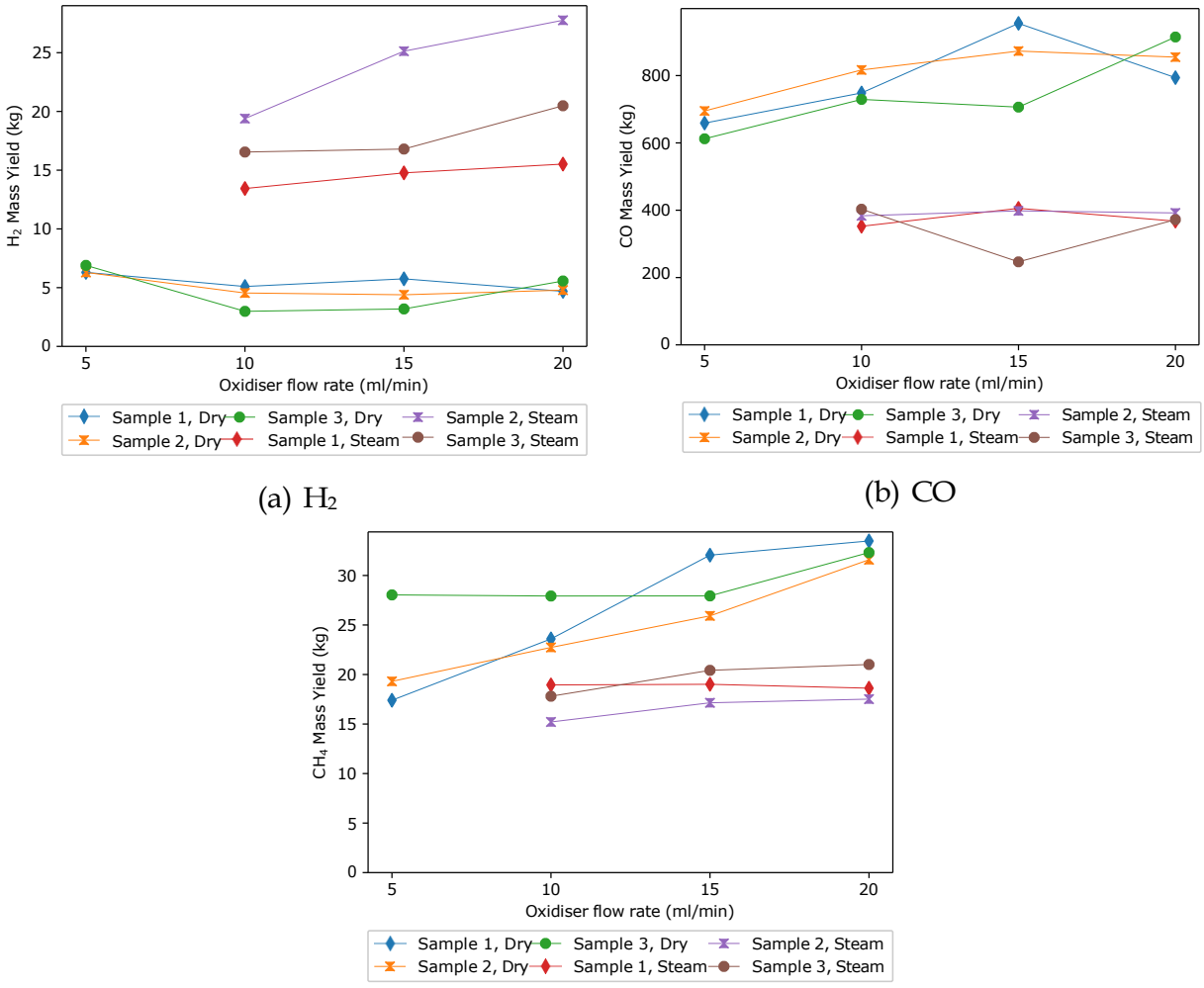

(a) H_2

(b) CO

(c) Methane

Figure 15: Mass of H_2, CO and methane produced from gasification of a full harvest

These results are directly proportional to the gas yields seen above in Figure 12 and show modest total yields of H_2 produced directly from the gasification process. The minimum amount produced was during dry gasification of Sample 3 with 10 ml min^{-1} of CO_2, and the maximum being produced during steam gasification of Sample 2 with 20 ml min^{-1} of Ar through the bubbler.

The mass of the H_2 and CO produced from reforming the methane obtained during gasification is shown below for each of the experiments in Figure 16.

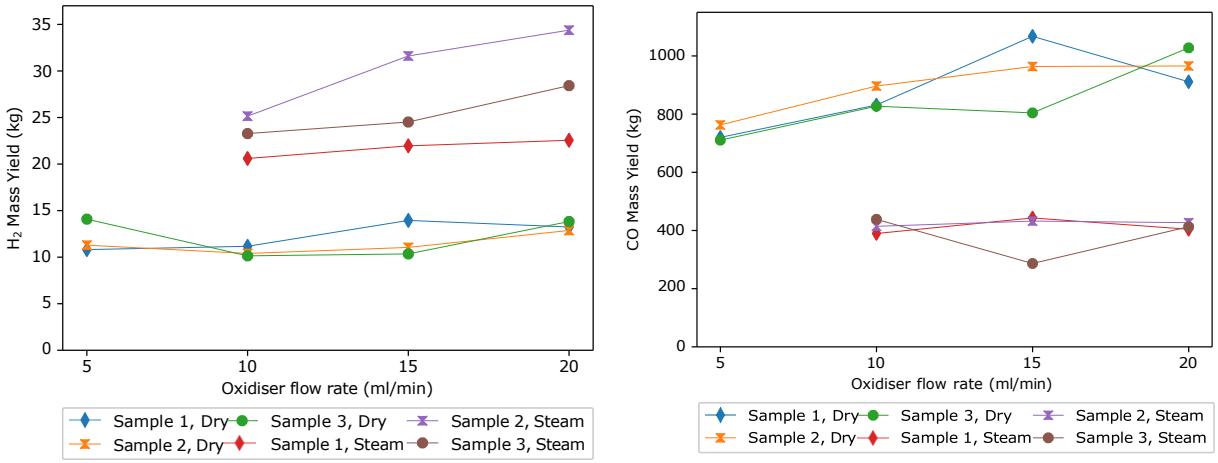

(a) H_2 (b) CO

Figure 16: Total mass of H_2 and CO produced with reforming of methane

4.6.2 Water Gas Shift

The amount of H_2 produced from conversion of the CO with the WGS reaction from one tonne of tomato vines is shown below in Figure 17.

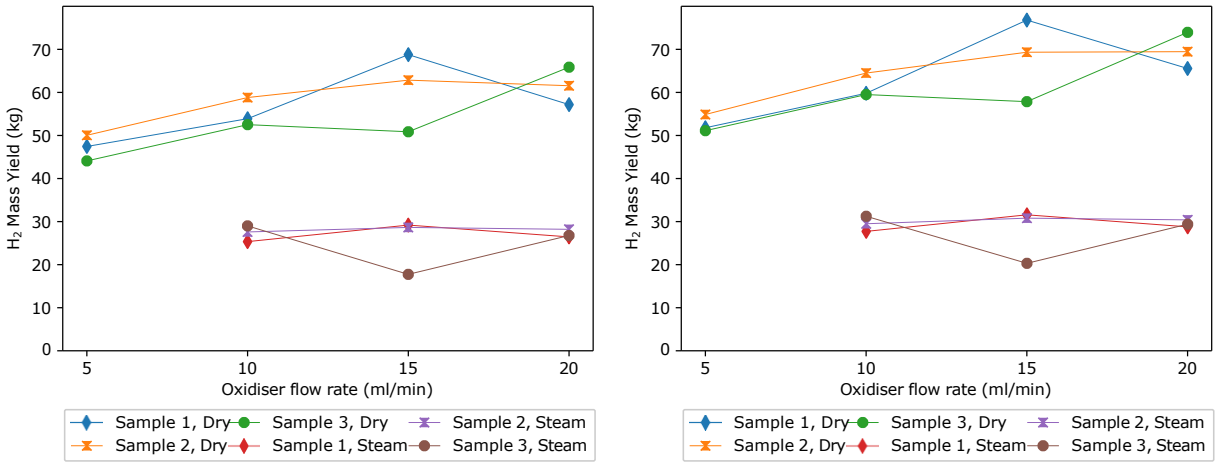

(a) Without methane reforming (b) With methane reforming

Figure 17: Mass of H_2 produced during the water gas shift reaction

The yield of H_2 produced from the WGS is proportion to the yield of CO seen above in Figures 15b and 16b, and is higher than the total H_2 produced from gasification and reforming directly. Whilst the WGS needs large amounts of H_2O and is performed at 400°C, it is exothermic meaning that the heat of reaction can be used to supply the latent heat of water and therefore the energy supply to this reactor is relatively small.

The highest yield obtained with reforming and the WGS reaction is approximately 77 kg of H_2 per tonne of vine gasified, which has an energy content of 3.03 MWh. This means that the total cost of harvesting, transportation and processing would have to be less than $385 tonne in order to compete with H_2 of prices of $5 kg^{-1} for H_2 produced with electrolysis.

As the large amounts of CO produced during dry gasification are fully converted into H_2 in the above figure, dry gasification combined with the WGS reaction has a higher H_2 yield than steam gasification. However, the production of this H_2 has a lower energy efficiency due to the need for the additional reactor and inputs to undertake the WGS reaction.

5 Conclusion

The gasification of agricultural wastes is considered an important source of renewable fuels [12], [13]. To understand the techno-economic feasibility of gasification of post-harvest residue, the yield quantity and quality of syngas obtained during gasification must be determined.

The composition of waste tomato vines was analysed and the syngas yield obtained in varied conditions was modelled using Aspen Plus®. These results were used to determine theoretical optimal temperature and oxidiser-flow conditions during gasification. Dry and steam gasification was undertaken in a lab-scale down-draft reactor and the composition of gases was recorded at short intervals.

Recorded data were analysed to determine the thermodynamic activity in the reactor during gasification. Increasing the ratio of oxidiser-to-biomass during the reaction improved the degree of gasification of the vine, but caused the WGS and RWGS reactions to occur during steam and dry gasification, respectively. The post-gasification residue present in the reactor was largely ash, and was of insufficient quantity to be analysed further for its use as a biochar.

The yield of H_2 obtained from 1 tonne of waste tomato vine is modest, with the highest mass produced from gasification, reforming and WGS being approximately 77 kg. Given the cost associate with harvesting the vines and pre-processing the vine waste for gasification, this process is unlikely to be cost competitive with other sources of green H_2 (eg electrolysis powered by renewables) which are well established technologies and more scalable. With significant global investment in electrolyser technology and the renewables that provide the electricity for green H_2, the cost of production for electrolysis derived H_2 are projected to decline further in the future. Furthermore, recent changes in processing tomato production systems have led to a per/ha reduction in the volume of vines post-harvest, which would increase the margin cost of collecting the vines from the paddock.

Due to these factors, the authors do not recommend moving to phase 2 for the project (full techno-economic viability assessment).

6 Bibliography

[1] J. Burgess, D. J. Batstone, T. H. Muster, and F. Pamminger, "Wastewater–an untapped resource?: Report of a study by the Australian Academy of Technological Sciences and Engineering (ATSE)," 2015.

[2] S. Shafiee and E. Topal, "When will fossil fuel reserves be diminished?" *Energy policy*, vol. 37, no. 1, pp. 181–189, 2009. doi: 10.1016/j.enpol.2008.08.016.

[3] P. De Luna, C. Hahn, D. Higgins, S. A. Jaffer, T. F. Jaramillo, and E. H. Sargent, "What would it take for renewably powered electrosynthesis to displace petrochemical processes?" *Science*, vol. 364, no. 6438, 2019. doi: 10.1126/science.aav3506.

[4] C. M. Plugge, "Biogas," *Microbial biotechnology*, vol. 10, no. 5, pp. 1128–1130, 2017. doi: 10.1111/1751-7915.12854.

[5] A. Henry, "Rethinking Waste Streams: New alternative for the Australian processing tomato industry," Tech. Rep., 2019.

[6] The Engineering ToolBox, *Fossil and Alternative Fuels - Energy Content*, 2008. [Online]. Available: https://www.engineeringtoolbox.com/fossil- fuels- energy-content-d_1298.html.

[7] R. Bader and W. Lipiński, "Solar thermal processing," in *Advances in Concentrating Solar Thermal Research and Technology*, Elsevier, 2017, pp. 403–459. doi: 10.1016/B978-0-08-100516-3.00018-6u.

[8] M. E. Dry, "The fischer–tropsch process: 1950–2000," *Catalysis today*, vol. 71, no. 3-4, pp. 227–241, 2002. doi: 10.1016/S0920-5861(01)00453-9.

[9] H. Mahmoudi, M. Mahmoudi, O. Doustdar, *et al.*, "A review of Fischer Tropsch synthesis process, mechanism, surface chemistry and catalyst formulation," *Biofuels Engineering*, vol. 2, no. 1, pp. 11–31, 2017. doi: 10.1515/bfuel-2017-0002.

[10] C. Agrafiotis, H. von Storch, M. Roeb, and C. Sattler, "Solar thermal reforming of methane feedstocks for hydrogen and syngas production—a review," *Renewable and Sustainable Energy Reviews*, vol. 29, pp. 656–682, 2014. doi: 10.1016/j.rser.2013.08.050.

[11] J. Wang and S. Wang, "Preparation, modification and environmental application of biochar: A review," *Journal of Cleaner Production*, vol. 227, pp. 1002–1022, 2019. doi: 10.1016/j.jclepro.2019.04.282.

[12] Ö . Tezer, N. Karabağ, A. Ö ngen, C. Ö . Ç olpan, and A. Ayol, "Biomass gasification for sustainable energy production: A review," *International Journal of Hydrogen Energy*, vol. 47, no. 34, pp. 15 419–15 433, 2022. doi: 10.1016/j.ijhydene.2022.02.158.

[13] C. T. Alves, J. A. Onwudili, P. Ghorbannezhad, and S. Kumagai, "A review of the thermochemistries of biomass gasification and utilisation of gas products," *Sustainable Energy & Fuels*, 2023. doi: 10.1039/d3se00365e.

[14] C. Higman, "Gasification," in *Combustion engineering issues for solid fuel systems*, Elsevier, 2008, pp. 423–468.

[15] Y.-J. Chang, J.-S. Chang, and D.-J. Lee, "Gasification of biomass for syngas production: Research update and stoichiometry diagram presentation," *Bioresource Technology*, p. 129 535, 2023. doi: 10.1016/j.biortech.2023.129535.

[16] O. of Energy Efficiency and R. Energy, *Hydrogen production: Biomass Gasification*, 2022. [Online]. Available: https://www.energy.gov/eere/fuelcells/hydrogen-production-biomass-gasification.

[17] Y. Zhang, L. Wan, J. Guan, Q. Xiong, S. Zhang, and X. Jin, "A review on biomass gasification: Effect of main parameters on char generation and reaction," *Energy & Fuels*, vol. 34, no. 11, pp. 13 438–13 455, 2020. doi: 10 . 1021 / acs . energyfuels . 0c02900.

[18] M. Ball and M. Wietschel, "The future of hydrogen–opportunities and challenges," *International journal of hydrogen energy*, vol. 34, no. 2, pp. 615–627, 2009. doi: 10.1016/j.ijhydene.2008.11.014.

[19] R. Hren, A. Vujanović, Y. Van Fan, J. J. Klemeš, D. Krajnc, and L. Čuček, "Hydrogen production, storage and transport for renewable energy and chemicals: An environmental footprint assessment," *Renewable and Sustainable Energy Reviews*, vol. 173, p. 113 113, 2023. doi: 10.1016/j.rser.2022.113113.

[20] U. Lucia, "Overview on fuel cells," *Renewable and Sustainable Energy Reviews*, vol. 30, pp. 164–169, 2014. doi: 10.1016/j.rser.2013.09.025.

[21] P. P. Edwards, V. L. Kuznetsov, W. I. David, and N. P. Brandon, "Hydrogen and fuel cells: Towards a sustainable energy future," *Energy policy*, vol. 36, no. 12, pp. 4356–4362, 2008. doi: 10.1016/j.enpol.2008.09.036.

[22] A. Poullikkas, "An overview of current and future sustainable gas turbine technologies," *Renewable and Sustainable Energy Reviews*, vol. 9, no. 5, pp. 409–443, 2005. doi: 10.1016/j.rser.2004.05.009.

[23] C. Tarhan and M. A. Ç il, "A study on hydrogen, the clean energy of the future: Hydrogen storage methods," *Journal of Energy Storage*, vol. 40, p. 102 676, 2021. doi: 10.1016/j.est.2021.102676.

[24] G. Mallouppas, C. Ioannou, and E. A. Yfantis, "A review of the latest trends in the use of green ammonia as an energy carrier in maritime industry," *Energies*, vol. 15, no. 4, p. 1453, 2022. doi: 10.3390/en15041453.

[25] S. Klinsrisuk, S. Tao, and J. Irvine, "Membrane reactors for ammonia production," in *Membrane reactors for energy applications and basic chemical production*, Elsevier, 2015, pp. 543–563. doi: 10.1016/B978-1-78242-223-5.00018-2.

[26] S. Ghavam, M. Vahdati, I. Wilson, and P. Styring, "Sustainable ammonia production processes," *Frontiers in Energy Research*, vol. 9, p. 34, 2021. doi: 10.3389/fenrg.2021.580808.

[27] Fertilizer Australia, *Australian Fertiliser Market*, 2023. [Online]. Available: https://fertilizer.org.au/about-fertiliser/the-fertiliser-industry/australian-fertilizer-market.

[28] IEA, "Ammonia Technology Roadmap," Paris, France, Tech. Rep., 2021. [Online]. Available: https://www.iea.org/reports/ammonia-technology-roadmap.

[29] W. David *et al.*, "Ammonia: Zero-carbon fertiliser, fuel and energy store," *Policy Briefing*, 2020.

[30] J. Ding, R. Ye, Y. Fu, *et al.*, "Direct synthesis of urea from carbon dioxide and ammonia," *nature communications*, vol. 14, no. 1, p. 4586, 2023. doi: 10.1038/s41467-023-40351-5.

[31] S. Simon Araya, V. Liso, X. Cui, *et al.*, "A review of the methanol economy: The fuel cell route," *Energies*, vol. 13, no. 3, p. 596, 2020. doi: 10.3390/en13030596.

[32] X. Cui and S. K. Kær, "A comparative study on three reactor types for methanol synthesis from syngas and CO2," *Chemical Engineering Journal*, vol. 393, p. 124 632, 2020. doi: 10.1016/j.cej.2020.124632.

[33] G. A. Olah, "Beyond oil and gas: The methanol economy," *Angewandte Chemie International Edition*, vol. 44, no. 18, pp. 2636–2639, 2005. doi: 10.1002/anie.200462121.

[34] K. Zhao, "A brief review of china's methanol vehicle pilot and policy," *Methanol Institute*, 2019.

[35] N. Shaari, S. K. Kamarudin, R. Bahru, S. H. Osman, and N. A. I. Md Ishak, "Progress and challenges: Review for direct liquid fuel cell," *International Journal of Energy Research*, vol. 45, no. 5, pp. 6644–6688, 2021. doi: 10.1002/er.6353.

[36] B. Ong, S. Kamarudin, and S. Basri, "Direct liquid fuel cells: A review," *International journal of hydrogen energy*, vol. 42, no. 15, pp. 10 142–10 157, 2017. doi: 10.1016/j.ijhydene.2017.01.117.

[37] M. P. Jones, T. Krexner, and A. Bismarck, "Repurposing Fischer-Tropsch and natural gas as bridging technologies for the energy revolution," *Energy Conversion and Management*, vol. 267, p. 115 882, 2022. doi: 10.1016/j.enconman.2022.115882.

[38] A. de Klerk, "Transport fuel: Biomass-, coal-, gas-and waste-to-liquids processes," in *Future Energy*, Elsevier, 2020, pp. 199–226. doi: 10 . 1016 / B978 - 0 - 08 - 099424 - 6.00012-0.

[39] J. S. Cha, S. H. Park, S.-C. Jung, *et al.*, "Production and utilization of biochar: A review," *Journal of Industrial and Engineering Chemistry*, vol. 40, pp. 1–15, 2016. doi: 10.1016/j.jiec.2016.06.002.

[40] K. Weber and P. Quicker, "Properties of biochar," *Fuel*, vol. 217, pp. 240–261, 2018. doi: 10.1016/j.fuel.2017.12.054.

[41] C. J. Ennis, A. G. Evans, M. Islam, T. K. Ralebitso-Senior, and E. Senior, "Biochar: Carbon sequestration, land remediation, and impacts on soil microbiology," *Critical Reviews in Environmental Science and Technology*, vol. 42, no. 22, pp. 2311–2364, 2012. doi: 10.1080/10643389.2011.574115.

[42] C. Steiner, "Biochar carbon sequestration," *University of Georgia, Biorefining and Carbon Cycling Program, Athens, GA*, vol. 30602, 2008.

[43] A. Mukherjee and R. Lal, "The biochar dilemma," *Soil research*, vol. 52, no. 3, pp. 217–230, 2014. doi: 10.1071/SR13359.

[44] D. Barlev, R. Vidu, and P. Stroeve, "Innovation in concentrated solar power," *Solar energy materials and solar cells*, vol. 95, no. 10, pp. 2703–2725, 2011. doi: 10.1016/j.solmat.2011.05.020.

[45] Y. Zhao, A. Dunn, J. Lin, and D. Shi, "Photothermal Effect of Nanomaterials for Efficient Energy Applications," in *Novel Nanomaterials for Biomedical, Environmental and Energy Applications*, Elsevier, 2019, pp. 415–434. doi: 10 . 1016 / B978 - 0 - 12 - 814497-8.00013-8.

[46] S. A. Said, M. Waseeuddin, and D. S. Simakov, "A review on solar reforming systems," *Renewable and Sustainable Energy Reviews*, vol. 59, pp. 149–159, 2016. doi: 10.1016/ j.rser.2015.12.072.

[47] H. Zhang, J. Baeyens, J. Degrève, and G. Cacères, "Concentrated solar power plants: Review and design methodology," *Renewable and sustainable energy reviews*, vol. 22, pp. 466–481, 2013. doi: 10.1016/j.rser.2013.01.032.

[48] HRL Technology Group Pty Ltd, *Specialist Engineering, Laboratory Testing, Innovation*, 2023. [Online]. Available: https://www.hrlt.com.au/.

[49] "Solid recovered fuels - Determination of moisture content using the oven dry method - Part 3: Moisture in general analysis sample," Swiss Association for Standardization (SNV), Winterthur, CH, Standard, 2021.

[50] "Solid recovered fuels — Determination of ash content," International Organization for Standardization (ISO), Geneva, CH, Standard, 2019.

[51] "Solid recovered fuels - Determination of content of volatile matter," Swiss Association for Standardization (SNV), Winterthur, CH, Standard, 2021.

[52] "Solid recovered fuels - Methods for the determination of carbon (C), hydrogen (H), nitrogen (N) and sulphur (S) by the instrumental method," Swiss Association for Standardization (SNV), Winterthur, CH, Standard, 2021.

[53] "Solid recovered fuels - Methods for the determination of sulphur (S), chlorine (Cl), fluorine (F) and bromine (Br) content," Swiss Association for Standardization (SNV), Winterthur, CH, Standard, 2011.

[54] "Standard Test Methods for Analysis of Wood Fuels," American Society for Testing and Materials (ASTM International), West Conshohocken, USA, Standard, 2019.

[55] Aspen Technology Inc, *Aspen Plus: Leading Process Simulation Software*, 2022. [Online]. Available: https://www.aspentech.com/en/products/engineering/aspen-plus.

[56] A. Demirbas, "Combustion characteristics of different biomass fuels," *Progress in energy and combustion science*, vol. 30, no. 2, pp. 219–230, 2004. doi: 10.1016/j.pecs. 2003.10.004.

Appendices

A Thermodynamic Analysis

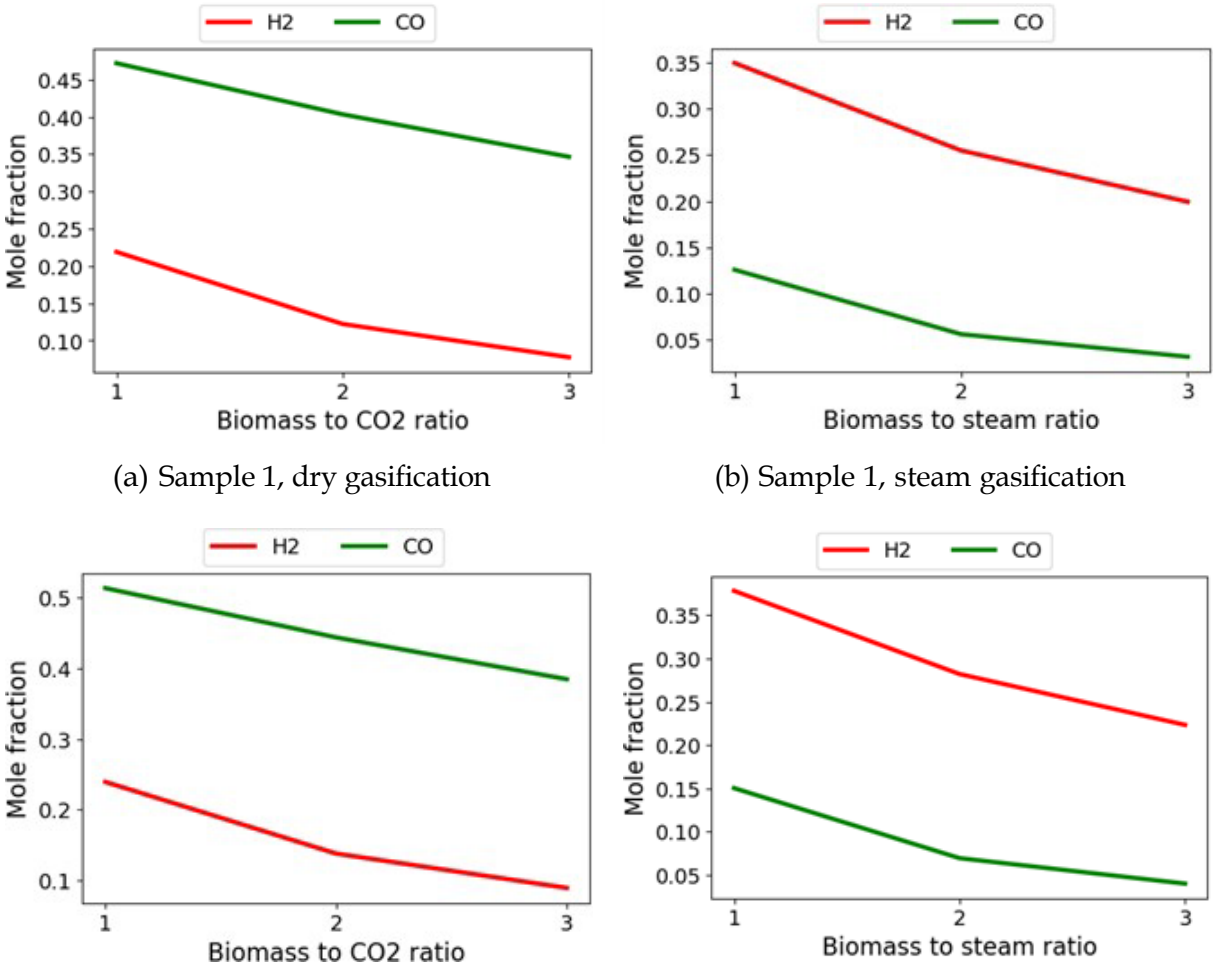

(a) Sample 1, dry gasification

(b) Sample 1, steam gasification

(c) Sample 3, dry gasification

(d) Sample 3, steam gasification

Figure 18: Molar fractions of H_2 and CO in the produced syngas for Samples 1 and 3

B Dry and Steam Gasification

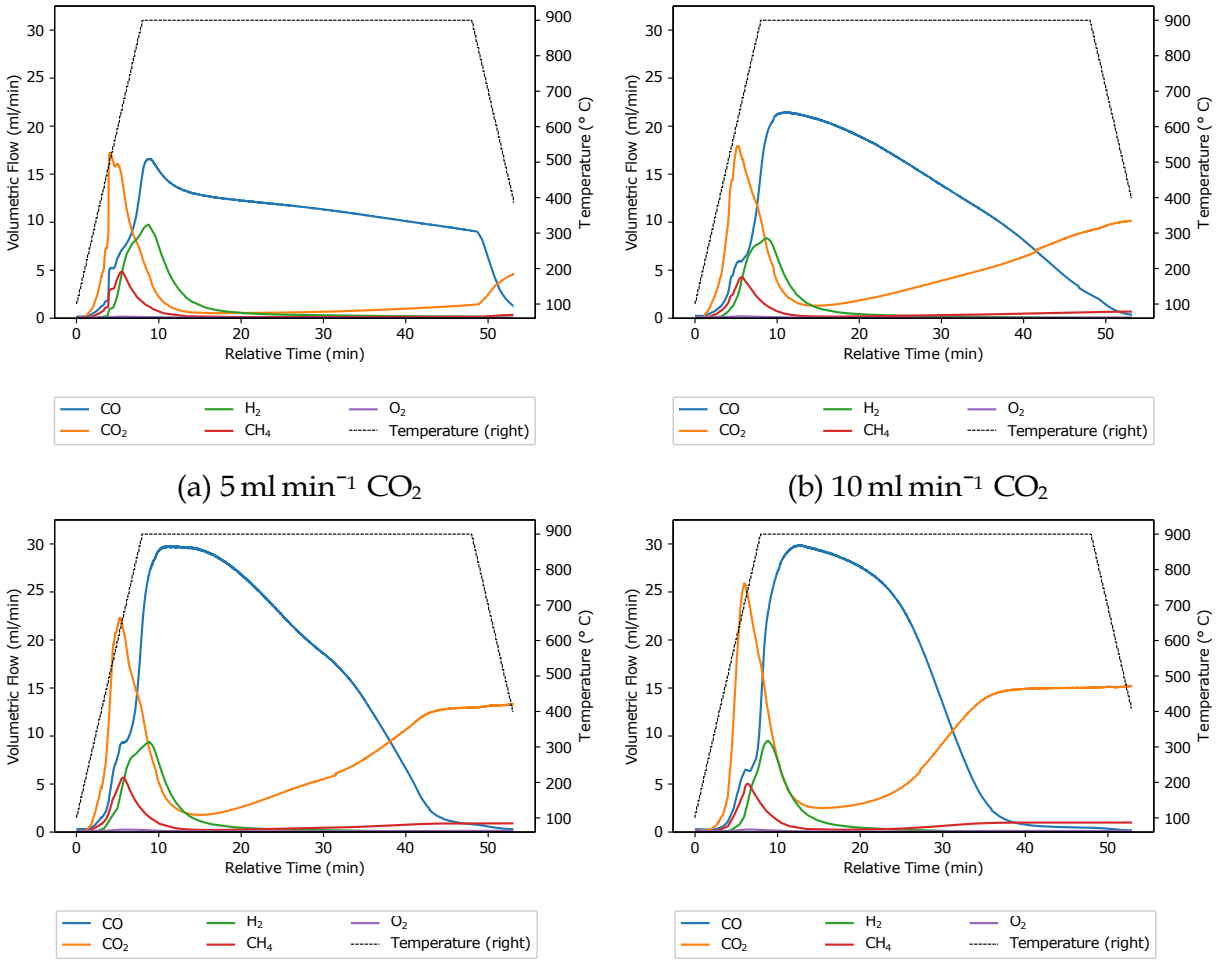

(a) 5 ml min^{-1} CO_2

(b) 10 ml min^{-1} CO_2

(c) 15 ml min^{-1} CO_2

(d) 20 ml min^{-1} CO_2

Figure 19: Flow rates of product gases recorded during dry gasification of Sample 1

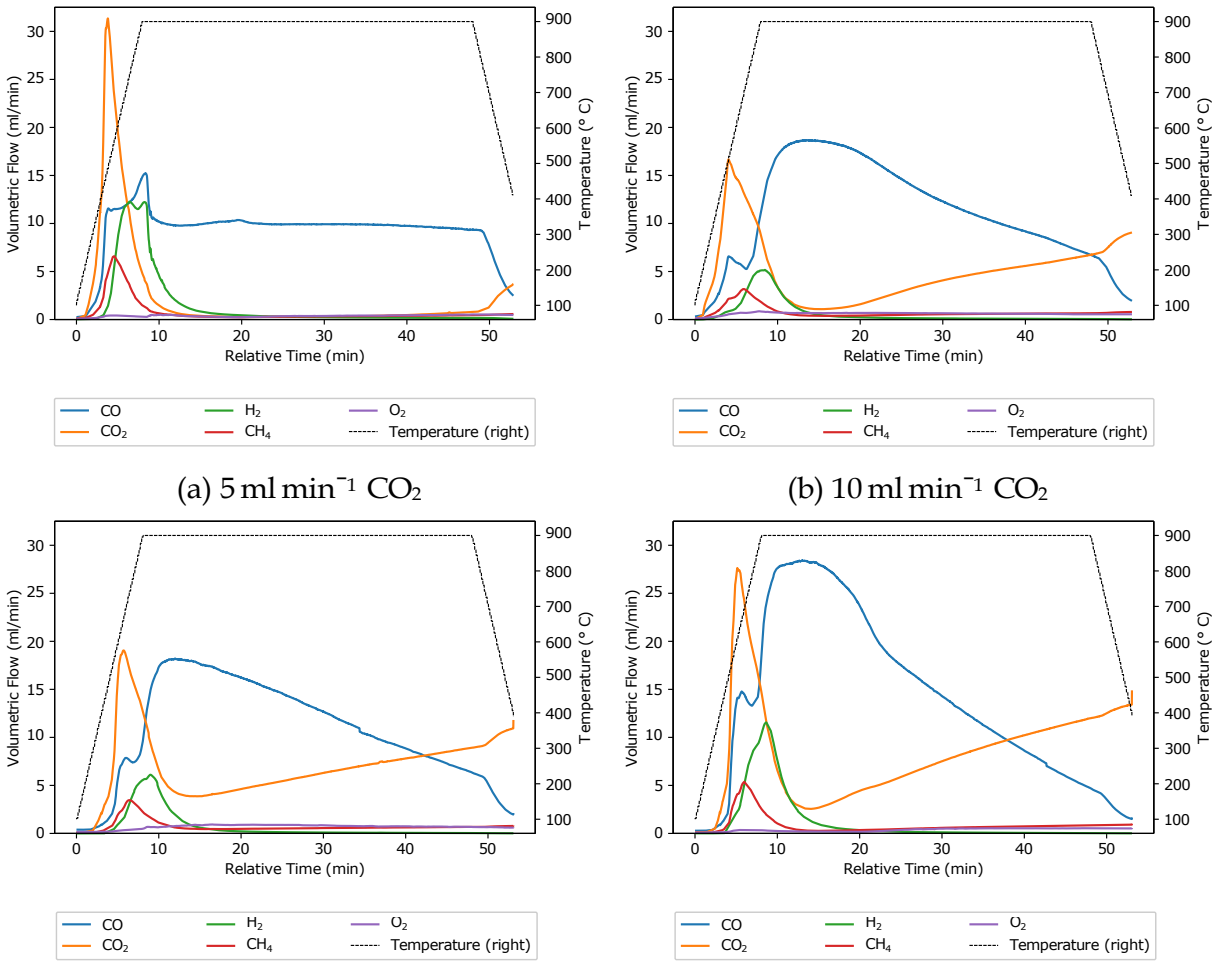

(a) 5 ml min^{-1} CO_2

(b) 10 ml min^{-1} CO_2

(c) 15 ml min^{-1} CO_2

(d) 20 ml min^{-1} CO_2

Figure 20: Flow rates of product gases recorded during dry gasification of Sample 3

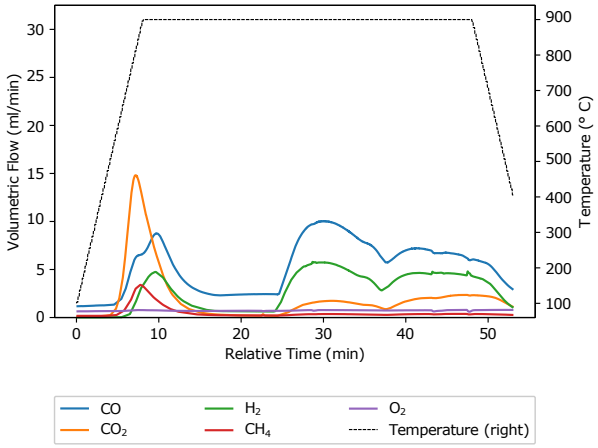

(a) 10 ml min^{-1} argon through bubbler

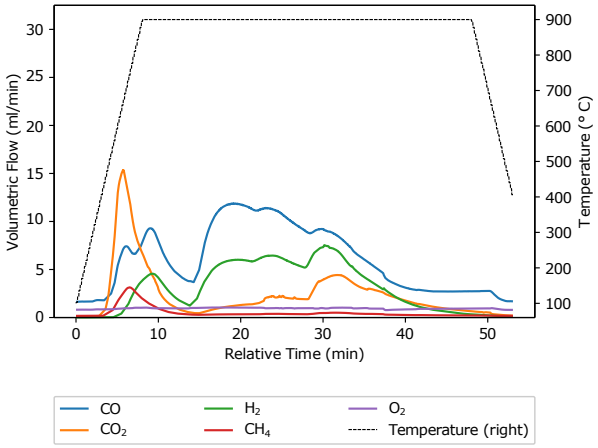

(b) 15 ml min^{-1} argon through bubbler

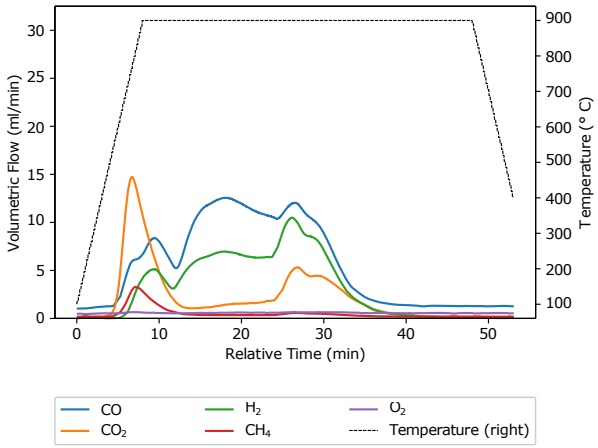

(c) 20 ml min^{-1} argon through bubbler

Figure 21: Flow rates of product gases recorded during steam gasification of Sample 1

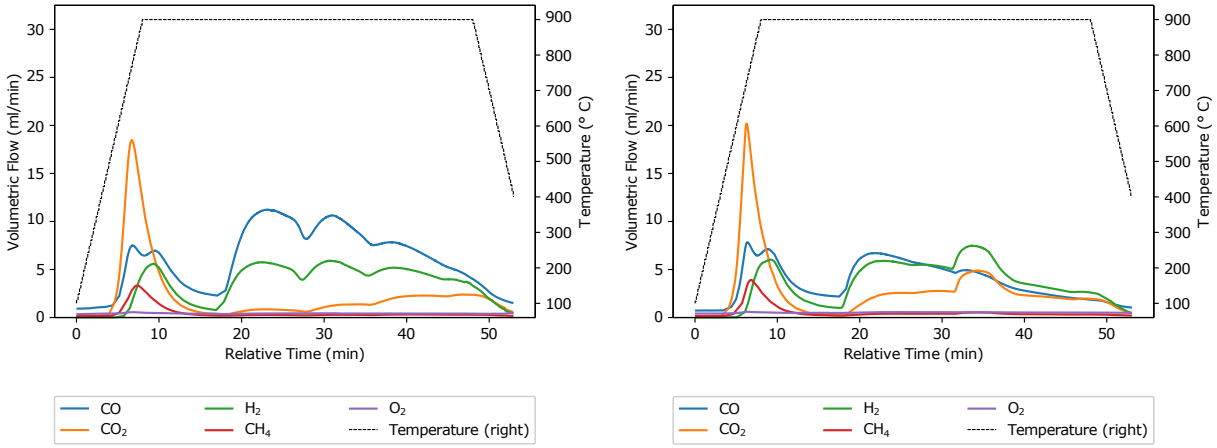

(a) 10 ml min^{-1} argon through bubbler

(b) 15 ml min^{-1} argon through bubbler

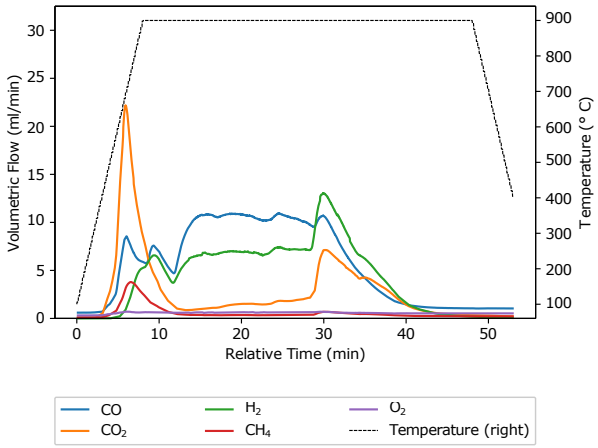

(c) 20 ml min^{-1} argon through bubbler

Figure 22: Flow rates of product gases recorded during steam gasification of Sample 3